SINGLE TRIAL ANALYSIS OF AUDITORY FMRI DATA

A Dissertation

Presented to

the Faculty of the Department of Electrical and Computer

Engineering

University of Houston

In Partial Fulfillment

of the Requirements for the Degree

Doctor of Philosophy

in Electrical Engineering

by

Xi Zhu

May 2012

Acknowledgements

I would like to express my deepest gratitude to my advisor Dr. Jansen for all the guidance and support he provided me throughout my study. I would also like to thank Dr. Sheth, Dr. Hiscock, Dr. Tsekos and Dr. Glover for serving as members of my dissertation committee. I am also thankful to Dr. Kayali for his technical assistance when I started this project.

Also, I would like to thank my parents (Junjie Zhu and Shufang Ma) and my friends in the lab (Xiaofei, David, Bharat, Deepa, Amol, Ruoli) for their support and encouragement. In addition, I would like to thank Dr. Bobbie Koen for spending time to discuss the research. I could not have done this without you.

SINGLE TRIAL ANALYSIS OF AUDITORY FMRI DATA

An Abstract

of a

Dissertation

Presented to

the Faculty of the Department of Electrical and Computer

Engineering

University of Houston

In Partial Fulfillment

of the Requirements for the Degree

Doctor of Philosophy

in Electrical Engineering

by

Xi Zhu

May 2012

Abstract

This research is concerned with functional magnetic resonance imaging (fMRI) of the brain during auditory information processing. The main focus is the exploration of the brain areas involved in sensory gating, i.e., the ability of the central nervous system (CNS) to inhibit or modulate its sensitivity to incoming irrelevant sensory auditory input, as measured using a paired auditory stimulus paradigm.

It is well-known that the brain's responses are variable from trial-to-trial. This calls into question the current practice of using a single, representative response function (canonical HRF) to model fMRI data. Therefore, a correlation-based method was developed to deal with the variability of the HRF in response to repeated presentation of identical auditory stimuli. The goal of the analysis technique is to identify 'active' trials among all single trials. We verified that this correlation-based method can find significant differences between brain areas and brain states in actual fMRI data.

Second, we determined if the cluster-based method can improve conventional fMRI analysis by exploring the brain regions involved in processing single stimuli using both methods. Data was collected from 14 healthy subjects listening to auditory tones. Our results indicated that by focusing on 'active' trials only, as determined by the clustering method, we obtained better statistical maps and that the sensitivity of the fMRI data analysis was increased through the identification of activated areas.

The results indicated that the superior temporal gyrus (STG), inferior frontal gyrus (IFG), dorsolateral prefrontal cortex (DLPFC), and thalamus (THA) were involved in auditory information processing and sensory gating in general. While the conventional analysis could not find any regions involved in gating, the correlation-based method confirmed the involvement of bilateral STG, right THA and left DLPFC in sensory gating. Specifically, the right THA relays the sensory signal to the STG, with the bilateral STG involved in the first stage of auditory processing and the left DLPFC involved in the inhibitory circuit of sensory gating processing.

Our findings suggest that the correlation-based single trial analysis method provides quantitative assessment of the neuronal origins of the sensory gating. It also improves the current fMRI analysis technique.

Table of contents

List of Figures

List of Tables

Chapter 1: Introduction

1.1 Background

1.1.1 Introduction to fMRI

Functional magnetic resonance imaging is a powerful noninvasive tool for the study of the functioning of the brain, which can provide high spatial resolution (on the order of millimeters) of activity in the brain resulting from sensory stimulation or cognitive function. It works by detecting the changes in blood oxygenation that occur in response to neural activity (Ogawa et al., 1990). Changes in the blood oxygenation level-dependent (BOLD) signal reflect neural activity, because firing neurons need more oxygen to be brought in quickly. This process is called the hemodynamic response.

Hemoglobin is diamagnetic (i.e., it is repelled by an externally applied magnetic field), when oxygenated but paramagnetic (i.e., it is attracted by a magnetic field) when deoxygenated. Putting an object with magnetic susceptibility into a magnetic field causes spin de-phasing, resulting in a decay of transverse magnetization which depends on the time constant T2*. (T2* is a measure of the loss of coherence in an ensemble of spins that include the effect of transverse relaxation caused by spin-spin interaction, T2, and changes in spin precession frequency of protons due to inhomogeneities in the magnetic field). The flipped oxyhemoglobin protons de-phase slower than the unflipped deoxyhemoglobin protons. Therefore, the T2* signal is retained longer in a region which has more oxygenated blood than regions

where there is less oxygenated blood. This change in signal intensity is called the blood oxygenation level dependent (BOLD) effect (Buxton, 2002; Huettel, 2004).

The BOLD signal can be measured in functional Magnetic Resonance Imaging (fMRI) scanners. Subjects participating in an fMRI experiment are asked to lie still in the scanner while they are subjected to sensory stimulation or participating in cognitive and/or behavioral experiments. Their head is usually restrained with soft pads to prevent movement; although small head movements can be corrected for in post-processing of the data, large transient motion cannot be corrected.

1.1.2 Variability of the fMRI signal

FMRI has a relatively poor signal-to-noise ratio. Therefore, functional brain imaging studies make use of ensemble-averaged activity over many trials and often across several subjects to enhance the signal-to-noise ratio of the small BOLD response hidden in the background noise. However, ensemble averaging may not be able to represent the true response from any single event, and it may obscure potentially significant inter- and intra- subject variability that may be important to capture. Actually, the BOLD signal has been found to show a large variability between subjects, sessions, and brain regions (Aguirre et al., 1998; Miezin et al., 2000).

The hemodynamic response variability can result from several factors. It has been known that the vascular response does not remain constant throughout the human brain because of the variability in vascular architecture

(Huettel et al., 2004). Study results have uncovered dissimilarities in different cortical regions within the individual brain or in different individuals (Buxton, 2002). In addition, other factors including global magnetic susceptibilities, neural activity differences, pulse of respiration differences or slice timing differences can also cause a variation in the hemodynamic response (Levin et al., 1998; Noseworthy et al., 2003).

1.1.3 Sensory gating

The ability of the brain to filter out repeated stimuli is referred to as sensory gating. Failure of the gating mechanism could lead to the central nervous system (CNS) being overloaded with irrelevant information and ultimately to a total dysfunction of the system (Freedman et al., 1991).

The gating capability is typically measured by the auditory paired-stimulus paradigm, in which P50 auditory evoked potentials (scalp-recorded) are measured (Adler et al., 1982). In a paired-stimulus paradigm, two identical stimuli (S1 and S2) are delivered with a short inter-stimulus interval of 500 ms and a longer inter-pair interval of 8 seconds. The second stimulus of a pair is suggested to be an irrelevant sensory input since it contains no new information. A decrement in the response to the second stimulus relative to the first is taken to indicate the operation of the gating out neural mechanism. Sensory gating is operationally defined as the ratio of the amplitude of the response to the second (S2) stimulus to the amplitude of responses to the first (S1) stimulus. In healthy subjects, responses to the second stimulus in the pair are suppressed compared to the first one. In contrast, subjects suffering from schizophrenia show a diminished inhibition of the responses to the

second stimulus (Adler et al. 1990; Boutros et al., 1991). Although the good temporal resolution of electrophysiological techniques allows for the disambiguation of S1 and S2 responses, these techniques are limited by their spatial resolution. Neuroimaging techniques such as fMRI, with higher spatial resolution and the ability to independently evaluate activation on a voxel-by-voxel basis, provide additional critical information on the role of the regions of interest such as prefrontal cortex and hippocampus in sensory gating.

1.1.4 SPM and General linear model (GLM)

Compared to many electrophysiological techniques, fMRI has a relatively poor signal-to-noise ratio (SNR). A very robust stimulus (such as a contrast taken between an auditory stimulus and no stimulus) may produce changes on the order of 2%-5% in the BOLD signal. The low SNR requires extensive post-processing and fMRI studies are always averaged over time and smoothed across space using Statistical Parametric Mapping (SPM). SPM was developed by the Welcome Trust Center for Neuroimaging for Matlab (Mathworks Inc). The objective of such analysis is to generate a brain image identifying the areas which present significant percentage signal change in response to the task. To estimate the BOLD signal in an experimental paradigm, the cross-correlation or *t* test within a general linear model (GLM) has been used (Friston et al., 1995).

The statistical analysis in SPM consists of a number of steps. First of all, the BOLD fMRI response must be modeled. Secondly, the parameters of this model must be estimated using GLM. Finally, it must be determined whether there is any evidence for a statistically-significant increase in the

BOLD fMRI response in response to a task condition. These processes normally need prior knowledge of the hemodynamic response and then proceed to explain the measured data by parameter estimation. SPM makes use of a canonical hemodynamic response function (HRF) to represent the hemodynamic response (HR) after neural activation. The canonical HRF in the SPM software package is a typical BOLD impulse response modeled by the difference of two gamma functions, one modelling the peak and one modelling the undershoot. As shown in Figure 1.1, the canonical HRF exhibits an increase peaking around 5 sec, followed by an undershoot that lasts for a considerable period.

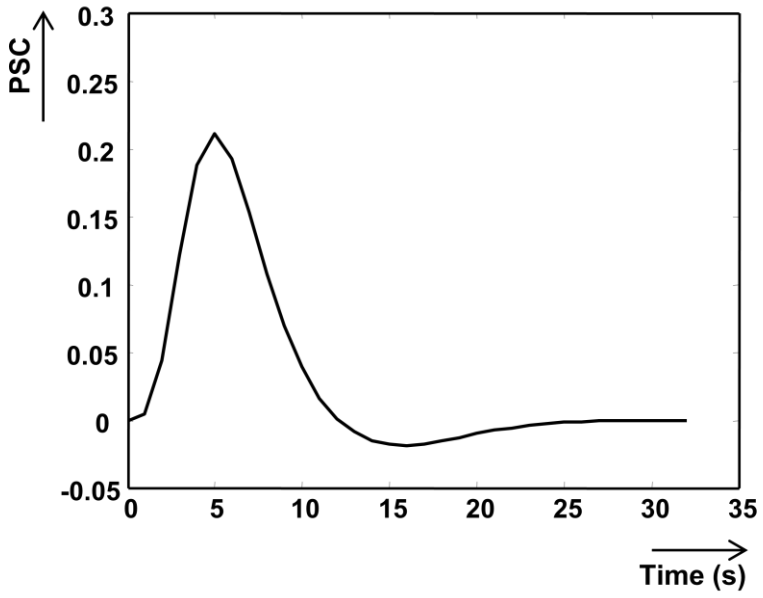

Figure 1.1: Canonical HRF as used in SPM. The y-axis is in percentage signal change (PSC), and the x-axis is in second.

Extensive statistical modeling, referred to as first-level analysis (see Appendix 1), is done to obtain t-statistic images that provide an indication

whether the response to the stimulus condition differ from a second one. When making inferences about the population, a second level analysis dealing with random effects can be implemented in SPM2 using the one-sample *t*-test function. The between subjects effect of diagnosis can be evaluated by entering parameter estimates from each individual's first level analysis into a second level model. Finally, the functional results can be overlaid onto the group averaged anatomical images for visualization.

1.2 Research Objectives

This research is concerned with functional magnetic resonance imaging (fMRI) of the brain during auditory information processing. The main focus is the exploration of the brain areas involved in sensory gating, as measured using a paired auditory stimulus paradigm. It is well-known (see 2.1) that the brain's responses are variable from trial-to-trial. Therefore, we will develop a cluster-based method to deal with this variability. This method will be evaluated on simulated and actual fMRI data. We will also show that it can improve conventional fMRI analysis, and that it can produce information not obtainable by conventional method. The specific tasks and studies to be performed include:

Specific Aim A: (Chapter 3) Development and evaluation of a single trial analysis method.

1. Development: Design and implement a correlation-based method to analyze single trial HRFs. The proposed clustering approach will use correlation as a measure of similarity between a template and single trials.

Trials with a high correlation coefficient with the template are grouped together and will be considered to represent ‘active’ trials, i.e., cases where a brain response to stimulation occurred. Then the ensemble average will be computed for each class, and the active subject-specific HRF can be obtained.

2. Evaluation: Determine the sensitivity of the cluster-based method using simulated and actual fMRI data obtained from different subjects and different brain areas.

First, the sensitivity of the cluster-based method will be assessed by analyzing “activated” brain regions, i.e., those from the auditory cortex, and “non-activated” brain regions, e.g., the visual cortex (occipital cortex) and comparing the activation levels. It is reasonable to assume that the auditory cortex will produce more responses to single auditory tones than the occipital cortex, and we will determine if the clustering method finds the same.

We also determine the sensitivity of the cluster-based method by analyzing different paradigm (e.g., listening to single tones or listening to double tones). Specifically, we expect that the auditory cortex produces more activation in response to double tones than single tones, and we will seek to confirm this with the clustering method.

Specific Aim B: (Chapter 4) Determine if the cluster-based method can improve conventional fMRI analysis.

This will be achieved by exploring the brain regions involved in processing single stimuli using conventional fMRI analysis, using data collected from healthy subjects listening to single tones. The same data will

be analyzed using the cluster-based method and the results will be compared. We expect that by focusing on ‘active’ trials only, as determined by the clustering method, we will obtain better statistical maps and that the sensitivity of the fMRI data analysis will be increased through the identification of activated areas with a low signal-to-noise ratio.

Secondary objectives will be to determine if a BOLD signal due to auditory stimuli can be robustly measured or not in the noisy MRI scanner using the conventional EPI sequence, which regions are involved in processing single and double stimuli, and which regions are involved in sensory gating in healthy subjects.

Specific Aim C: (Chapter 5) Acquiring new knowledge using the single-trial method.

Use the new method to examine sensory gating and test whether we can provide more information than conventional fMRI analysis. First, we will re-examine the sensory gating network by using active trials only, and comparing the results with conventional analysis. Second, a string-based analysis will be carried out to examine the cooperation between these ROIs. This method assigns a string of zeros and ones to each trial, indicating which ROI was active (encoded by a one) and which was not (encoded by a zero). These strings can then be searched to determine if a particular pattern of active/non-active ROIs is more prevalent for the single tone experiments than the double tone experiments, thus providing insight in what activation patterns are characteristic for gating and which are not.

1.3 Dissertation outline

Chapter 2 presents a review of previous work done on fMRI analysis. This includes the studies of BOLD signal variability, methods for modeling the hemodynamic response and fMRI studies of auditory sensory gating. Chapter 3 presents the developed cluster based methods followed by an evaluation of this method using simulated data and real fMRI data. Chapter 4 presents the comparison between the cluster-based method and the conventional fMRI analysis. In chapter 5, the correlation-based method is applied to investigate sensory gating network. Finally, Chapter 6 summarizes the findings and offers conclusions for this study.

Chapter 2: Literature Review

The first two sections of this chapter review the literature on the studies pertinent to the variability of the BOLD hemodynamic response and modeling the hemodynamic response of fMRI data. The third section discusses the ROI analysis methods. The fourth section reviews the fMRI studies on auditory sensory gating in healthy and schizophrenia subjects.

2.1 Variability of BOLD Hemodynamic response

Several groups have indicated that hemodynamic responses to visual stimuli differ from subject to subject (Boynton et al., 1996; Kim et al., 1997; Aguirre et al., 1998) and that responses appear to be more stable during a single scanning session within a single subject (Kim et al., 1997; Aguirre et al., 1998). For example, Aguirre et al. (1998) found that the inter-individual variations in the peak latency and magnitude can be as large as 3.5 s and 2%, respectively, in the hemodynamic responses from the central sulcus. However, little variability within the same subject across different days or scanning sessions was found. This was confirmed by Menz et al. (2006) using prolonged (120 min) functional measurements. Relatively small differences have also been observed in the HRF from different brain regions of the same subject (Buckner et al., 1996; Miezin et al., 2000; Neumann et al., 2003; Handwerker et al., 2004). For example, Buckner et al., (1996) noted a delay of 0.5-1 s between visual and prefrontal regions.

Therefore, any application of the GLM using the canonical HRF may not be appropriate as it assumes that the BOLD response is invariant

between trials. Such variance due to regional or inter-subject differences in the HR can be reduced by individual-specific modeling or voxel-specific modeling which creates a single GLM with a specific HRF for every subject or ROI (Josephs et al., 1997).

In this study, we will quantify the inter-subject and intra-subject BOLD response variability to auditory stimuli using the new proposed cluster-based model. To the best of our knowledge, this is the first study to quantify the BOLD variability in the auditory fMRI field.

2.2 Modeling Hemodynamic Response

Function shapes that are typically used to model the HRF as the canonical hemodynamic response include the Poisson function (Friston et al., 1994), the Gaussian function (Rajapakse et al., 1998), spine-like function (Gossl et al., 2001), Fourier basis functions (Josephs et al., 1997) and the gamma function used as SPM's canonical HRF (Friston et al., 1998). These functions are usually selected prior to the analysis and assumed fixed over time and through brain regions. Given the relatively higher stability of the hemodynamic response observed within a single subject, a promising analysis approach is to predict the hemodynamic response information from the measured data for every subject, and then use that subject-specific response to further analyze BOLD fMRI data from that subject. These methods have been termed "recognition models", and include the selective averaging method (Anders et al., 1997), deconvolution method (Lu et al., 2006, Wink et al., 2008), principal component analysis-PCA (Hossein et al.,

2003), and the Bayesian method (Ciuciu et al., 2003; Marrelec et al., 2003). The merit of recognition models lies in the power of estimating the subject-specific or even region-specific HRF. If such an approach is followed, much better results can be obtained.

For example, Aguirre et al. (1998) compared the use of the Poisson function (Friston et al.. 1994), the gamma function (Boynton et al., 1996), and an empirical subject-specific HRF. Aguirre et al. (1998) found that the Poisson function, on average, explained only 25% of the variance present in the evoked responses, and the gamma model accounted for 70% of the variance. In contrast, subject-specific models on average explained nearly 92% of the variance.

Kang et al. (2003) compared the activated areas and *t*-statistical scores obtained with a standard HRF to those obtained with a patient-specific HRF. The activated areas obtained with the patient-specific HRFs were larger or similar to the originally activated areas. The results show that using patient-specific HRFs brings increased sensitivity to the analysis of epileptic spikes by EEG-fMRI.

Lu et al. (2006) introduced a deconvolution method for EEG-fMRI activation detection, which can be implemented with voxel-specific HRFs. A comparison of performance was made between three fixed HRFs and the deconvolution method. The authors found that the volume of detected regions from the deconvolved HRFs was larger, and the deconvolution technique found areas of activation that were not detected with the three fixed HRFs.

Several problems remain with modeling the HRF: (1) some methods use fixed HRFs assuming that the shape of the hemodynamic response is known a priori and invariant throughout the brain and subjects. This is a strong constraint since it is known that HRFs can vary as a function of brain region, age, and gender. (2) It is often assumed that the HRFs are identical from one response to another which is unlikely to be the case (Aguirre et al., 1998). (3) Some methods obtained the subject-specific HRF by projecting the actual fMRI signal onto a Fourier basis which is probably only a rough approximation of the BOLD response.

The HRF cluster method to be developed here has the advantages that (1) It is data-driven instead of model-driven. It does not rely on any assumptions of the HRF: the extracted HRFs are determined only by the fMRI signal and the stimuli and it is not biased by any a priori model. (2) In this method, no assumption is made that all the single trials are the same. Thus the proposed method can provide a more complete picture of the different kinds of HRFs that may exist during an experiment. (3) No rough approximation is needed in this method. The subject-specific HRFs described here are derived from the clusters of data itself. (4) In addition, this method has the advantage of simplicity compared to the methods described above, since all the calculations are done within GLM. Finally, the proposed cluster method removes the non-active trials which can increase the signal to noise ratio (SNR).

2.3 ROI analysis

In complex designs with more than two conditions, it can often be difficult to detect the patterns of activity across conditions from an overall map (Poldrack, 2007). However, in case we know where the activation is likely to be, it is often useful to see the signal in regions of interest (ROI) plotted for each condition or plotted against other variables of interest. So we will first need to define an ROI, and then analyze the data within the ROI.

A key problem in an ROI analysis is to define the right ROI. There exists substantial variability between individuals in the shape and location of anatomical regions, and the relationship between function and anatomy is very unclear in many regions of the brain, especially the prefrontal and association cortex. One approach to address this issue is to use the individual's own activation pattern to define the ROIs for each subject and use this ROI to analyze other scans from the same subject. This approach is called functional ROI (Saxe et al., 2006; Heller et al., 2006). However, it requires that the functional data used for defining the ROI is independent of data used to test the hypotheses of interest on the ROIs. In other words, it needs extra scans to identify which voxels in a particular anatomical region represent a particular response.

Another approach is to use a group-defined functional ROI instead of an individual's ROI. This means selecting functionally-activated voxels from the group results and using those voxels as an ROI to extract information from individuals. The activated voxels in the group will have some activation in most subjects. Also this method requires less processing time than

individually-defined ROIs. However, these group-level ROIs are not as reliable as the individually-created ones (Swallow et al. 2003) since it does not take into account the inter-individual functional variability.

The third approach is to a priori define a set of anatomical ROIs, and then measure the signal within the entire ROI (Tregellas et al., 2007). Regions specified in this approach will be relatively large (e.g., the entire superior temporal gyrus), and even if the region is significantly active, maybe only a small proportion of the voxels in the ROI is activated. By averaging across the entire ROI, the signals could be cancelled out. This approach also assumes that the particular region is functionally homogeneous and it does not consider that the subregions may behave differently.

This suggests that using the subject's own activation pattern to define the subject-specific ROI within main anatomical ROIs will be a good choice. This will compensate for inter-subject anatomical variability and offer better localization. Further the number of activated voxels in each region can be counted and compared between different conditions. (Poldrack et al., 2007)

Another key problem in ROI-based analysis is how to calculate an overall summary measure of the response in a ROI. There are two types of measurements used to quantify brain activation. The first one is to calculate the number of activated voxels (NAV) that exceeds a pre-defined statistical threshold (Wang et al., 2011). The NAV offers a spatial measurement to quantify the degrees of activation in a cortical ROI (Luft et al., 2002). This method has been used in many neuroimaging studies (Carey et al., 2002; Brodtmann et al., 2007; Pell et al., 2008).

The second one is to measure the averaged image intensity (AII) in a ROI. This approach decreases the noise since AII averages the image intensity across certain voxels, and it leads to making inferences about the response of the ROI as a whole rather than specific voxels within the ROI. In general, there are three main methods to obtain the AII of a ROI.

The first is called peak-averaging. In this case, signals are extracted from the voxels that have maximum activation and the average response is obtained. This provides a set of exploratory spheres that span the clusters of interest. The spheres are often masked with the thresholded statistical parametric map to ensure that they only contain voxels that are truly activated. This method is biased and the underlying assumption is that the ROI is homogeneous and the activation patterns are the same across all the voxels within this ROI.

The second method is called first eigenvariate. Principal components analysis (PCA) is applied to the region data, and the first eigenvariate is obtained. PCA is a mathematical procedure that uses an orthogonal transformation to convert a set of observations of possibly correlated variables into a set of uncorrelated variables, referred to as principal components. The time points are the observations and the voxels are the variables. Each component is associated with a vector of weights reflecting the contribution of each voxel to that component. The first eigenvariate reflects the time course of the main component that contributes to a ROI's response. However, the same problem exists as with peak-averaging, namely, that the eigenvariate may only reflect a small portion of the ROI, rather than the overall region's

response if the area is not homogeneous. In that case, the spatial weights of the component must be analyzed carefully. The most common method is the thresholded-average approach which averages the response across all the voxels passing a pre-determined threshold within the ROI. The advantage of this approach is that it can adapt flexibly to detect regions with almost any size or shape (Saxe et al., 2006). This method will be applied in this study.

2.4 fMRI studies of auditory sensory gating

Both animal and invasive human neuroimaging techniques (Boutros et al., 2005; Grunwald et al., 2003) suggest that sensory gating is mediated by a network including the auditory cortex (AC), prefrontal cortex and hippocampus. In contrast, the majority of results from non-invasive electrophysiological studies have not implicated the prefrontal cortex and/or hippocampus in gating (Mayer et al., 2009).

Despite the noisy environment of the scanner, hemodynamic correlates of auditory stimuli have been successfully recorded by several research groups (Mayer et al., 2009; Inan et al., 2004; Tregellas et al., 2007). Inan et al. (2004) compared two identical 1000 Hz tones (100 ms duration) separated by one, four, or six-second inter-stimulus intervals (ISIs) with 17 to 20 s between single or pairs of tones, and reported both a smaller amplitude and delayed onset to the second of each pair of stimuli at all ISIs. It is unclear to what degree this reflects sensory gating as the intra-pair intervals exceeded those used in the paired stimulus paradigm. They also observed that the response to repeated stimuli caused the allocation of additional neural resources.

Tregellas et al. (2007) investigated the neuro-anatomical substrates of sensory gating deficits in schizophrenia using fMRI. This study involved 12 schizophrenia patients and 12 healthy subjects while performing a sensory gating task. Hemodynamic responses were obtained utilizing a click-train paradigm in which nine clicks were presented over a 4-second interval, each 0.5 s apart, respectively. Comparing these responses with healthy subjects, schizophrenia patients had greater activation in the hippocampus, thalamus and dorso-lateral prefrontal cortex than healthy subjects. No group difference was found in the superior temporal gyrus. Mayer et al. (2009) examined the effects of distinct, compared to repeated, paired stimuli by using pairs of identical (first tone: 2000 Hz; second tone: 2000 Hz) and non-identical tones (first tone: 2000 Hz; second tone: 3000 Hz). In addition, single tones of the same two fundamental frequencies (2000 Hz or 3000 Hz) were used as a control non-gating condition. The empirical HRFs were obtained from paired-tone responses. The estimated HR was obtained from a HRF for the single-tone conditions to which the same HRF delayed by 500 ms was added. The estimated HRF serves as a control non-gating condition. The authors used the estimated HRFs compared to the empirically determined HRFs to identify regions that exhibited gating responses for both identical and non-identical paired-tone. Results indicated that the gating response for both paired-tone conditions was primarily mediated by the auditory and prefrontal cortex, with potential contributions from the thalamus. Results also showed that the left auditory cortex may play a preferential role in determining the stimulus to be inhibited (gated) or to receive further processing due to novelty of information. In contrast, there was no evidence of hippocampal involvement. These fMRI

studies suggest that a network including the superior temporal gyrus (STG), prefrontal cortex (PFC), thalamus (THA) and hippocampus (HPC) involved in sensory gating. Chapter 4 investigates which ROIs mentioned above contribute to sensory gating using conventional analysis, and chapter 5 provides further analysis of sensory gating using the correlation-based method. Chapter 6 provides a summary of the major findings, a critical review of the results and a look at the future.

Chapter 3: Methods and Sensitivity Evaluation

In this chapter, we present a data-driven method to extract the active single trials from fMRI time series, based on a clustering technique. In section 3.1, we give the flowchart of the overall procedure, and the details of the analysis steps. In section 3.2, the performance assessment of the method using simulated data is presented, and an evaluation using actual fMRI data is presented in section 3.3.

3.1 Development of the Analysis Technique

The goal of the analysis technique is to identify ‘active’ trials among all single trials. In this context, an active trial is the one showing a response to an external stimulus. The overall procedure is presented in the Figure 3.1. Briefly, a correlation-based method is used to identify groups of trials with similar post-stimulus characteristics on a trial-by-trial basis. Correlation is used as a measure of similarity between a template, resembling activity typically-associated with robust fMRI responses, and single trials. Trials that show a high correlation with the template are grouped together as active trials. Then the ensemble average is computed for each class, resulting in the active subject-specific HRF and/or active region-specific HRF. A detailed description is presented next.

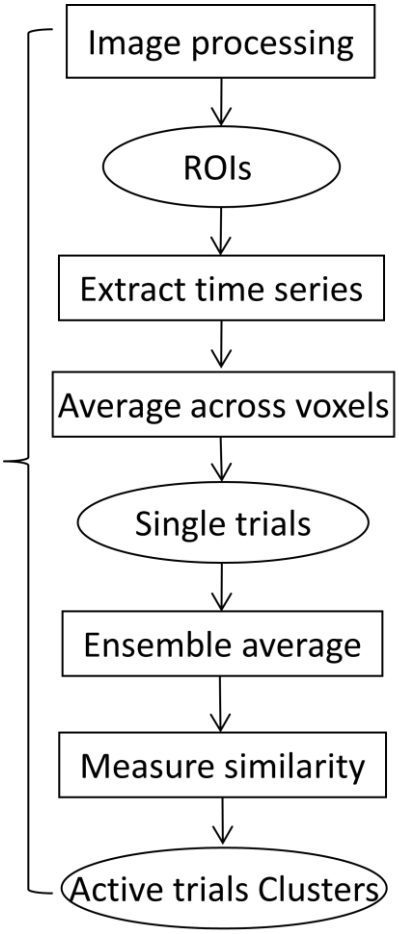

Figure 3.1: Flowchart of analysis procedures.

The template is obtained as follows. The group-averaged statistical maps of all subjects are generated using the canonical HRF. The main areas of activation at $p \leq 0.001$ during processing of single tones are found and the time series within the ROIs are extracted and ensemble averaged across all voxels in the ROIs. A 32 s discrete cosine transform (DCT) is applied to remove low-frequency noise introduced by unavoidable factors like scanner drift and physiological processes. The 16 s signal following stimuli delivery is taken as the single trial response. The timeseries are normalized to percentage signal change and all the single trials as well as the ensemble averaged HRFs are adjusted to set the value of the first sample of the time

window to zero for display purposes. The ensemble average across all the single trials is used as the template.

The correlation between the template and each single trial over the fixed window of 2 s - 8 s post-stimulus is computed. This window was selected because the hemodynamic responses reach their peak in this interval, and the signal-to-noise ratio will thus be maximal. The correlation R_i for trial *i* is given by

$$R_i = \frac{\sum_n h_T(n) h_i(n)}{s_T s_i}, \tag{3-1}$$

where $h_T(n)$ is the template hemodynamic response, $h_i(n)$ represents the single trial *i*, and s_T and s_i are the standard deviation of the template and single trial, respectively.

Two criteria need to be met by a single trial response to be classified into the active group. First, the correlation between the single trial and the template must exceed a certain threshold (e.g., 0.5). Second, the standard deviation (STD) of the single trial within the window [2s 8s] must be greater than a threshold. The first criterion ensures the selection of trials that are similar in shape to the template, while the second criterion ensures that the activation level is sufficiently large. Experiments were conducted on simulated and actual data to determine an acceptable correlation threshold and STD threshold.

Each of the trials from a specific ROI can be labeled as active (1) or non-active (0) using the clustering method. Combining the results across

ROIs, each trial can be represented by a string of characters. The strings are equal in length to the number of ROIs, and each character in the string identifies the type of response seen for the corresponding ROI. For example, the string ‘1001’ could mean that the STG is active, the DLPFC is not, the IFG is not, and the THA is active. These strings can be searched to see if a particular pattern of active/non-active ROIs is more prevalent for one paradigm than another.

3.2 Performance evaluation on simulated data

3.2.1 Data generation

Simulated data were generated using data obtained from an auditory fMRI experiment in which fourteen healthy subjects were listening to single auditory pure tones of 1000 Hz (4 ms in duration with a 2 ms rise and fall time) in the scanner. The auditory cortex was selected as the ROI, and the 0 s to 8 s interval of each trial following stimulus presentation was considered ‘active’, while the 8 s to 16 s intervals were considered as ‘non-active’ responses. The reason to use 0-8 s windows as the active responses is that BOLD signal normally peaks 4-6 s after stimulus begins, and the BOLD signal will have basically died out during the 8-16 s interval. To verify that a response was present or not, the ensemble average for each of the two groups was computed. Next, ten ‘active’ responses were randomly selected and ensemble-averaged to generate one new ‘active’ response and this was repeated until 500 new ‘active’ responses were obtained. The same

procedure was applied to the non-active group of trials. Figure 3.2 shows the trials thus generated.

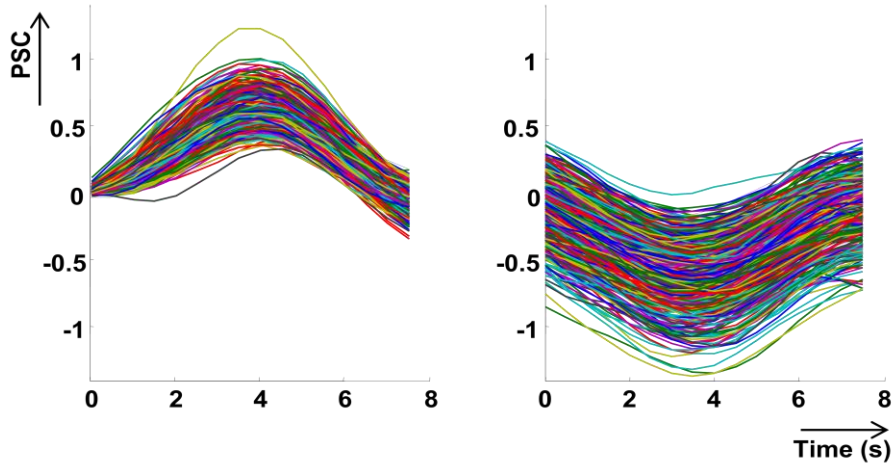

Figure 3.2: Left panel: simulated 'active' responses; right panel: 'non-active' responses.

Noise was added to the simulated responses with different signal-to-noise ratios. The residual error of ε in the GLM (see Eq. A1-2) was used to simulate the noise. The reason not to use white noise is that the noise in fMRI is complicated. The sources of noise include intrinsic thermal noise, system noise, artifacts resulting from head motion and physiological processes, variability in neuronal activity associated with non-task-related brain processes, and changes in behavioral performance and cognitive strategy (Huettel et al., 2004).

The time series were extracted and averaged across all voxels in auditory cortex. A 32 s DCT filter with cut-off frequency 0.03 Hz was used to remove low frequency component from the signal and GLM was applied to all 14 subjects. Figure 3.3 presents the power spectrum of an fMRI time series averaged across voxels in a specific ROI from one subject. The averaged

spectrum (Bartlett Method) was obtained to reduce estimation variance and improve measurement accuracy. The spectrum shows a clear peak at 0.057 Hz, corresponding to the frequency with which the auditory stimuli were presented, i.e., once per 16 to 18 s (0.0556 to 0.0625 Hz). The power spectrum of the residual error for the same subject after GLM was applied is also shown in Figure 3.3. As expected the peak frequency was suppressed.

A total of 1000 noise segments of 8 s in length were randomly selected from the residual error obtained from 14 subjects. The ensemble average of these noise segments is presented in Figure 3.4 (left panel) and the power spectrum was computed for each segment and averaged, with the result also shown in Figure 3.4 (right panel). As one can see, the noise is canceled out in the time domain and the averaged power spectrum is extremely small.

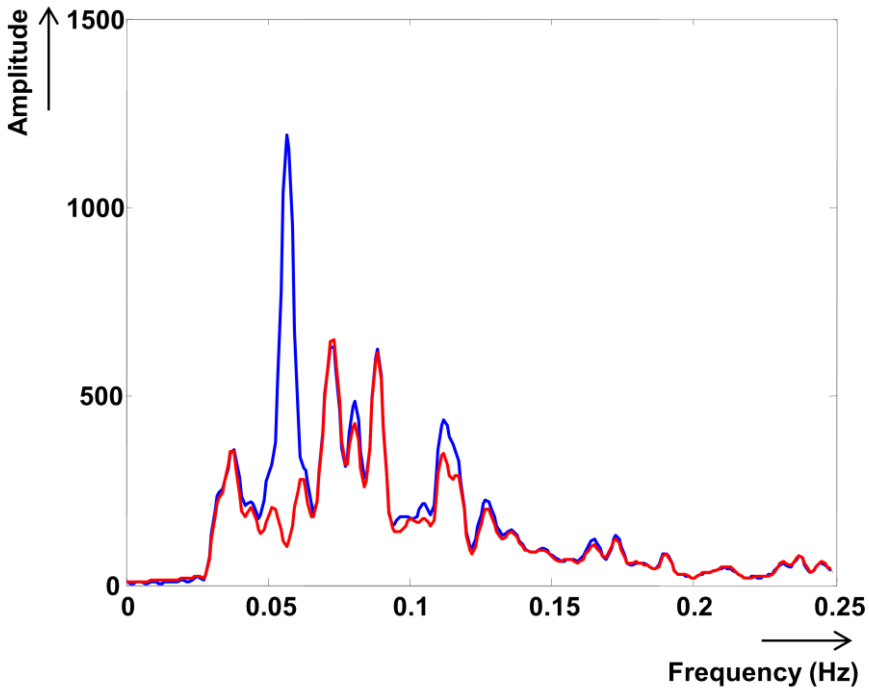

Figure 3.3: Power spectrum of time series (blue) and residual error (red) for one subject.

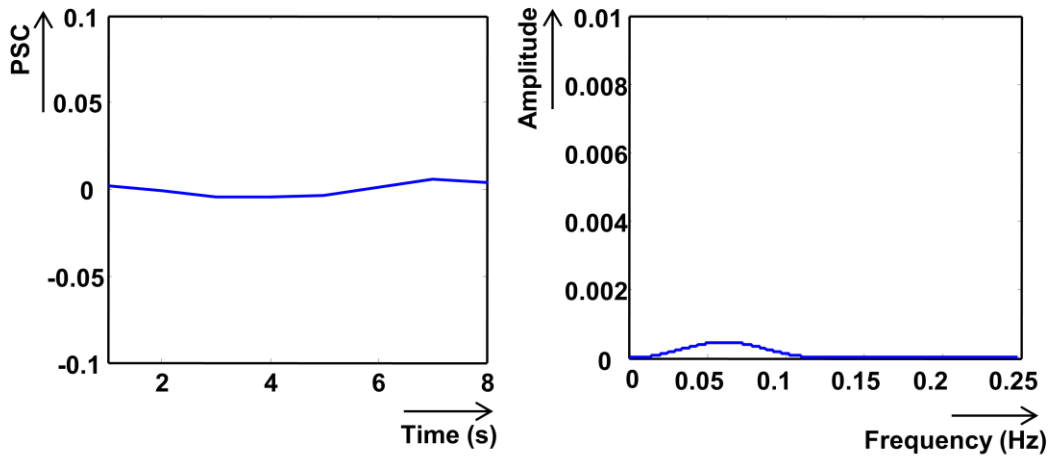

Figure 3.4: The averaged signal of 1000 noise segments (left panel) and the averaged power spectrum of the noise (right panel).

3.2.2 Sensitivity evaluation

The effect of Signal-to-Noise Ratio (SNR) on the clustering results was studied. SNR is defined as the ratio between the power in a signal (meaningful information) and the background noise (unwanted signal). We selected SNRs ranging from 0.1 to 4 to match noise levels seen in fMRI (Huettel et al., 2004). The noisy trials were classified using varying correlation thresholds and STD criteria. The number of correctly and incorrectly classified trials was obtained and a confusion matrix (see Table 3.1) was generated for each SNR/correlation threshold/STD criterion.

Table 3.1: Confusion matrix. TP: True Positives, FP: False Positives, TN: True Negatives, and FN: False Negatives.

		Test Result	
		1	0
True status	1	TP	FN
	0	FP	TN

Traditionally, the sensitivity and specificity are used to measure the performance of the test and they are defined as

$$\text{Specificity (TNR)} = TN / (TN + FP), \tag{3-2}$$

$$\text{Sensitivity (TPR)} = TP / (TP + FN), \tag{3-3}$$

where TP stands for true positives, FP indicates false positives, TN denotes true negatives, and FN false negatives. However, in our case, we seek to identify a set of single trial responses that are most likely ‘active’, i.e., we want to minimize the number of false positives, while maximizing the true positives. Therefore we seek to maximize the true active rate (TAR) defined by

$$TAR = TP / (TP + FP). \tag{3-4}$$

The correlation between single trial and template, and the STD were obtained for all single trials, including both active and non-active trials, at different SNR levels. Figures 3.5 through 3.7 show the scatter plot at SNR 4, SNR 0.5 and SNR 0.2, respectively.

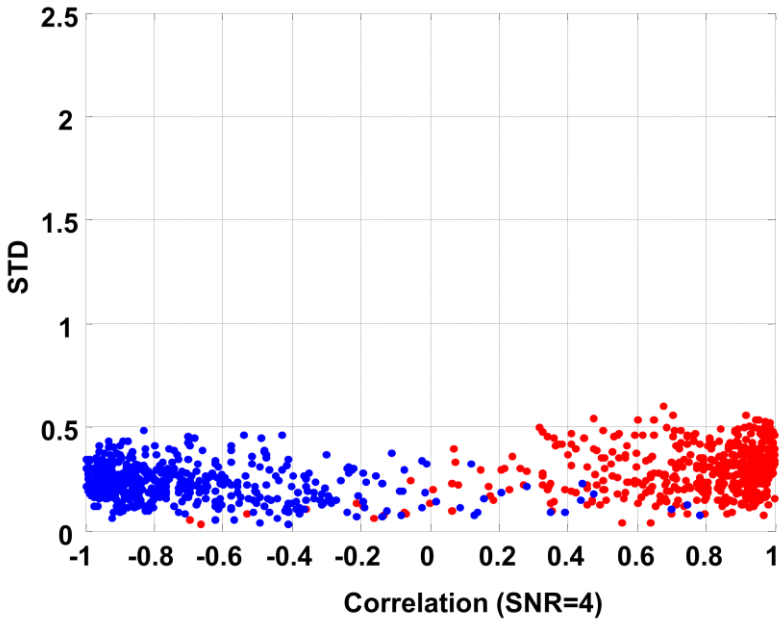

Figure 3.5: Scatter plot (correlation versus STD) of all single trials at SNR=4. Red dots: active trials; blue dots: non-active trials.

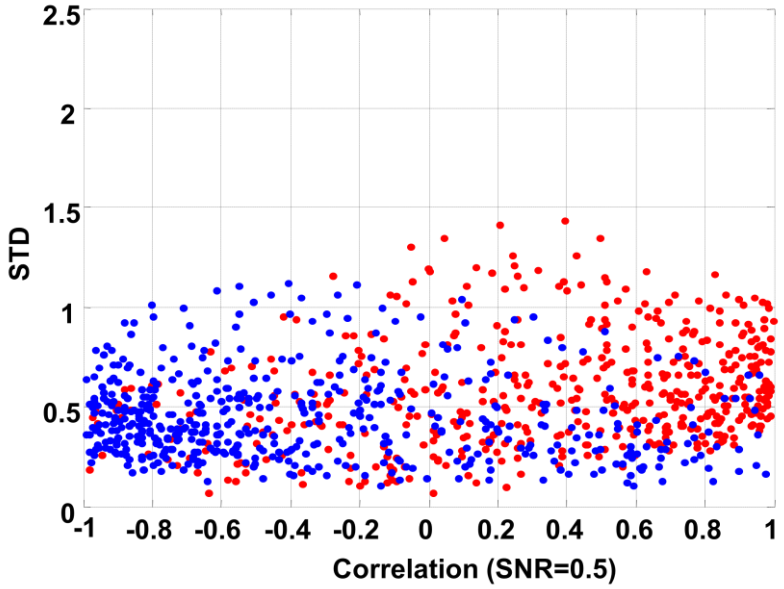

Figure 3.6: Scatter plot (correlation versus STD) of all single trials at SNR=0.5. Red dots: active trials; blue dots: non-active trials.

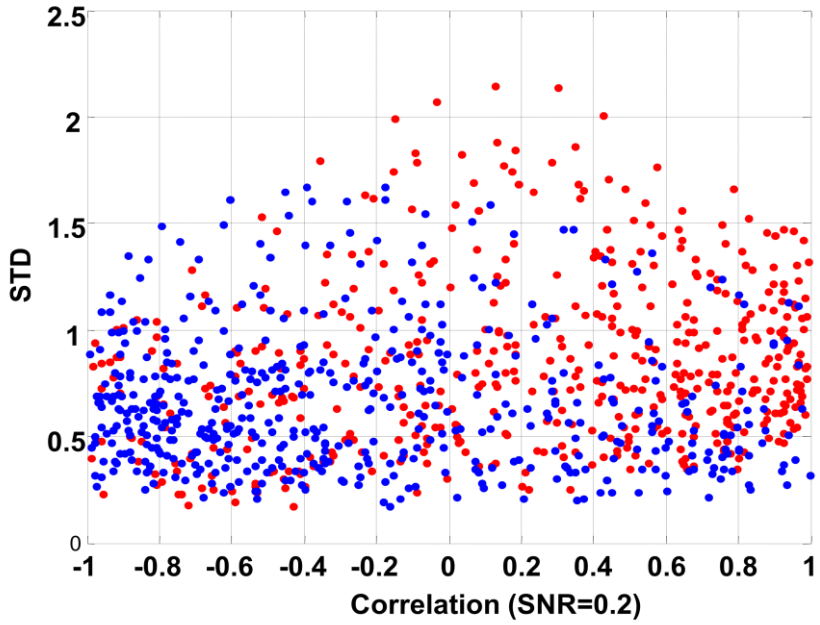

Figure 3.7: Scatter plot (correlation versus STD) of all single trials at SNR=0.2. Red dots: active trials; blue dots: non-active trials.

These figures show that at high SNR, the active and non-active trials could almost be perfectly separated on the basis of the correlation coefficient. As the SNR decreased, the two groups of trials become less and less separable. Also, the STD range increased from [0 0.5] to [0 2.3] as the SNR decreased. Furthermore, it appears that active trials at the high end of the correlation scale have a somewhat larger STD than inactive trials with similar correlation values.

By way of an example, the template for the active group using a SNR equal to 0.5 is shown in Figure 3.8. All single trials with cross-correlation larger than 0.5 with this template and STD larger than the STD of the template were clustered into the active group, and all other single were clustered into the non-active group. The clustering results are shown in Figure 3.9, and the corresponding confusion matrix is presented in table 3.2.

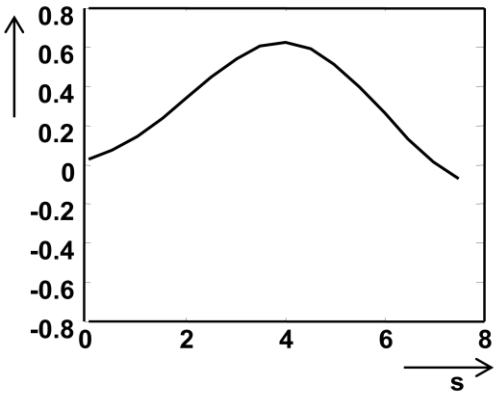

Figure 3.8: Template for active group at SNR=0.5.

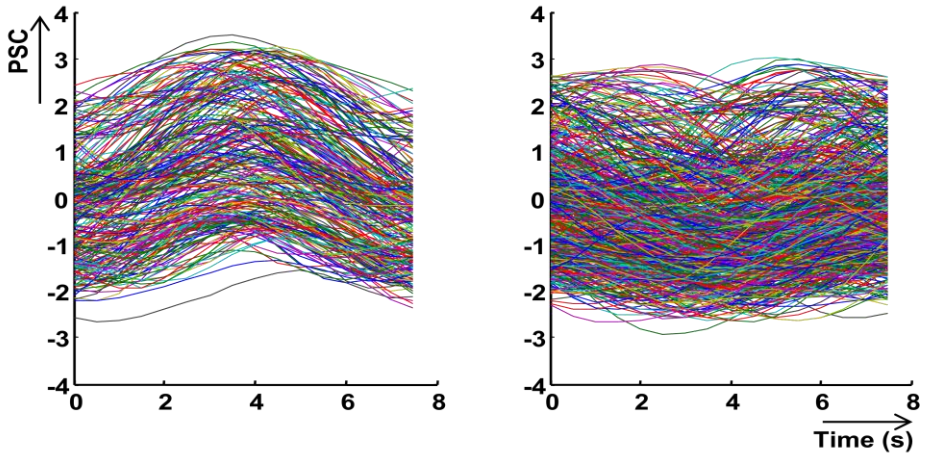

Figure 3.9: Clustering results with correlation threshold 0.5 at SNR=0.5; left panel: active cluster; right panel: non-active cluster.

Table 3.2: Confusion matrix at SNR=0.5, Threshold=0.5.

SNR=0.5		prediction outcome		
		T1(A)	T2(NA)	total
actual value	1	242	258	500
	0	56	444	500
	Total	298	702	1000

The specificity (TNR) for this example is 88.8% (444/500) and the sensitivity (TPR) is 48.4% (242/500). In our case, we seek to identify a set of single trial responses that are most likely ‘active’, i.e., we want to minimize the number of false positives, while maximizing the true positives. Thus, for the

case shown in Table 3.2, The TAR is 81% (242/298) which indicate 81% of the trials classified as ‘active’ where truly active, with 19% TNR (56/298) trials incorrectly assigned to the active group. At the same time, we also want to maximize TPR, which guarantees we can find enough active trials.

As mentioned before, different brain areas have different SNR values. This requires us to evaluate our method using different SNRs. Our experiment was repeated for different SNRs from 0.1 to 4. Different correlation thresholds from 0.1 to 0.9 and difference STD value from minimum STD to four times the STD of the template among all single trials were also evaluated.

First, experiments were done keeping the STD criterion fixed, but varying the SNR from 0.1 to 4. The correlation threshold was varied from 0.1 to 0.9 and the STD threshold was set to that of the template (0.235). The TAR and TPR were obtained and the results are presented in Figure 3.10.

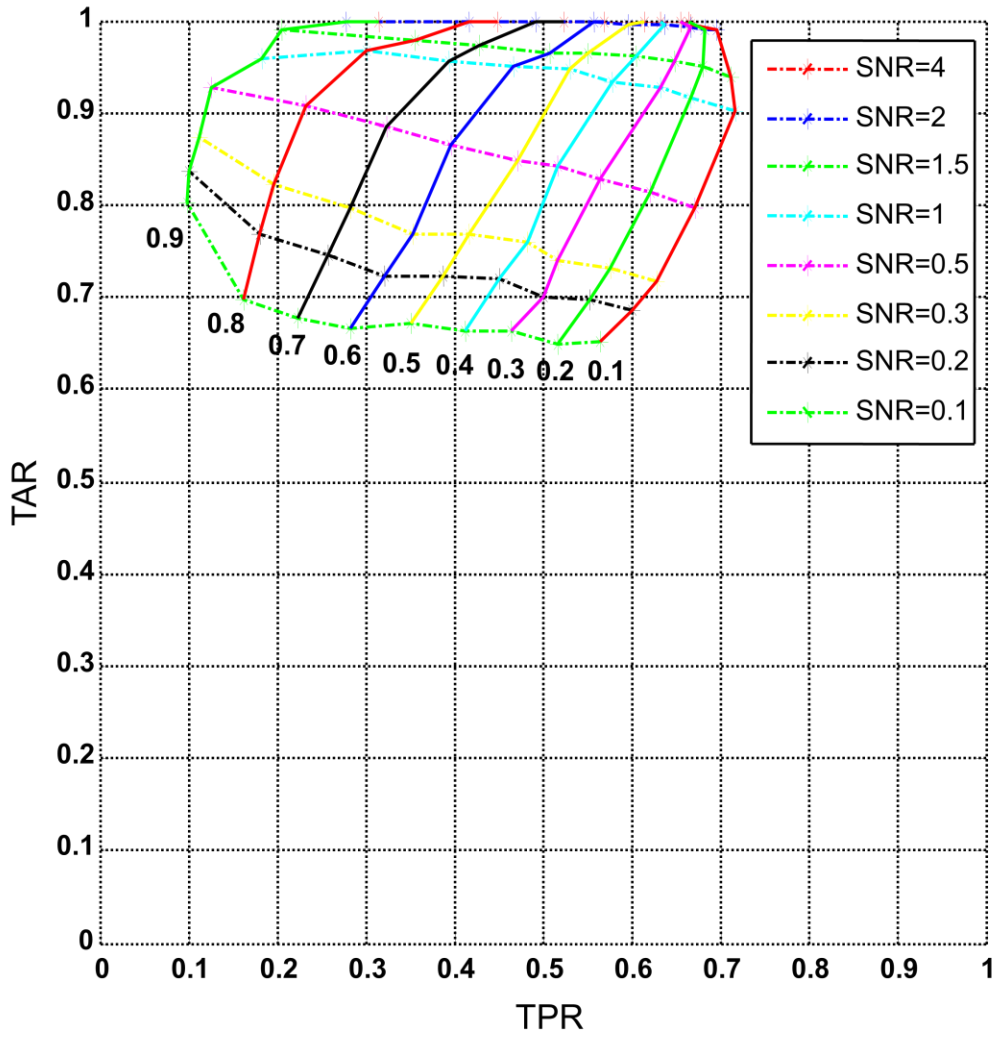

Figure 3.10: True active rate (TAR) and True positive rate (TPR) for different SNRs and correlation thresholds (red number) at STD = 0.235.

The result shows that the TAR was not sensitive to the threshold, but the TPR was sensitive to the threshold at certain SNR. For example, at SNR=1, when the threshold varied from 0.1 to 0.9, the TAR only varied from 90% to 96%. However, the TPR decreased from 71% to 18%. This means by using a large threshold we can get a higher TAR (96%), while ending up with very few active trials (18%). This suggests the use of a lower threshold which can guarantee an acceptable TAR, while maintain a relatively high TPR.

Figure 3.10 will be used to set the correlation threshold once the SNR has been determined for the fMRI data to be analyzed.

Next we studied the effect of the STD threshold, while keeping the correlation threshold fixed. To obtain a realistic correlation threshold the SNR was estimated from our auditory experiment as follows. The GLM was applied and the residual was taken to represent the noise. The signal power was obtained by computing the mean square value of the ensemble averaged time series from all voxels in the STG. The average SNR across all subjects was found to be 0.23. By using correlation threshold criterion only, we can achieve a 73% TAR (235/322) and 47% TPR (235/500) at correlation threshold = 0.4. Next, we assessed whether the STD could be used to improve the TAR while maintain the same TPR.

Data with a SNR of 0.23 were generated, and clustering was done with a correlation threshold of 0.4. The STD of the template is 0.235. The TAR and TPR were obtained by varying the STD from minimum STD (0.15) to four times of the STD of the template. The results are shown in Figure 3.11.

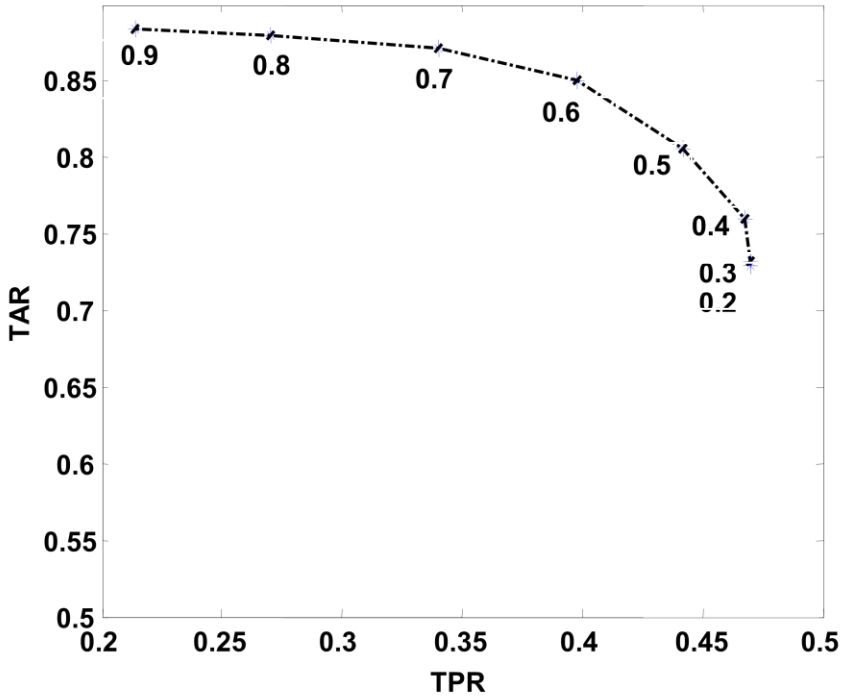

Figure 3.11: TAR and TPR for different STD thresholds at fixed SNR (0.23) and fixed correlation threshold (0.4).

As mentioned before, the STD threshold needs to be selected such that we obtain the largest possible TAR while having the largest number of true actives. The TAR did not improve when STD below 0.3 was used. As the STD increased from 0.3 to 0.9, the TAR increased from 73% to 88%, at the same time, the TPR decreased from 47% to 21%. Therefore, we need to consider the tradeoff between TAR and TPR. When we choose the STD equal to two times the standard deviation of the template (around 0.5), TAR will be increased from 73% to 81%, while the TPR only decreases from 47% to 44%.

Therefore, we decided to use an STD threshold of 0.5, which is around two times the standard deviation of the template. The active trials obtained by

applying these two criteria (STD>0.5; threshold = 0.4) fall in the orange box shown in Figure 3.12.

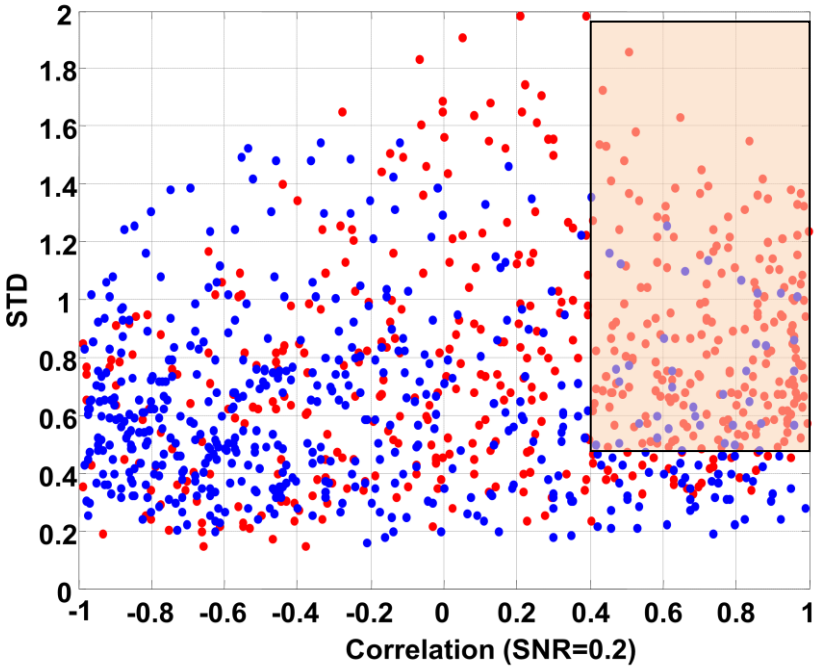

Figure 3.12: Scatter plot of all single trials at SNR=0.2 with two criteria STD>0.5; and threshold =0.4. Red dots: active trials; blue dots: non-active trials. The active trials by applying the criteria fall in the orange box.

3.3 Evaluation using actual fMRI data

Here we test if the correlation-based method can find differences between brain areas and conditions.

3.3.1 Comparison between visual and auditory cortex

It is reasonable to assume that the auditory cortex will produce more responses to *single* auditory tones than the occipital cortex, and we will determine if the clustering method finds the same.

FMRIs were obtained from 14 healthy subjects listening to auditory pure single tones of 1000 Hz (4 ms in duration with a 2 ms rise and fall time). A 16 s interval between events was used to guarantee that the BOLD responses had returned to baseline before the next stimulus was presented. The main area of activation was the auditory cortex (AC) which was selected as the 'active' dataset (Figure 3.13). This area included 438 voxels. The averaged time series across voxels was calculated for each subject. A DCT filter with cut-off frequency 0.03 Hz was used to remove the low frequency noise. Nearly 50 trials were available for each subject, and a total of 566 single trials were obtained across all subjects (Figure 3.14 left panel). The single-trial HRFs were normalized to percentage signal change and Figure 3.14 (right panel) shows the average signal of all the 566 single trials. This collection of single trials HRFs is referred to as the 'active' dataset.

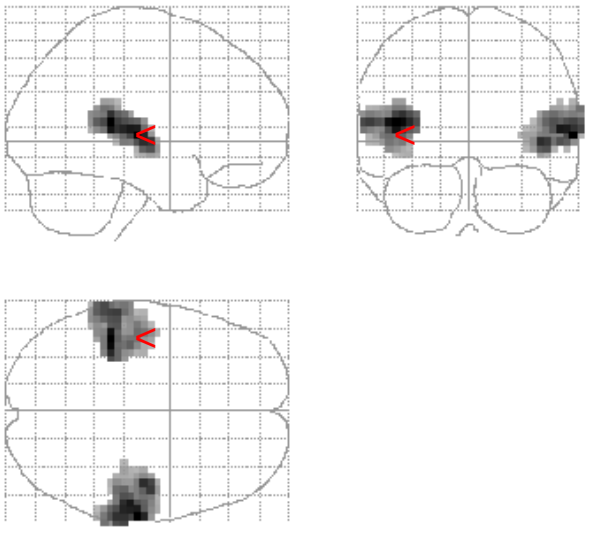

Figure 3.13: Statistical maps for the auditory cortex.

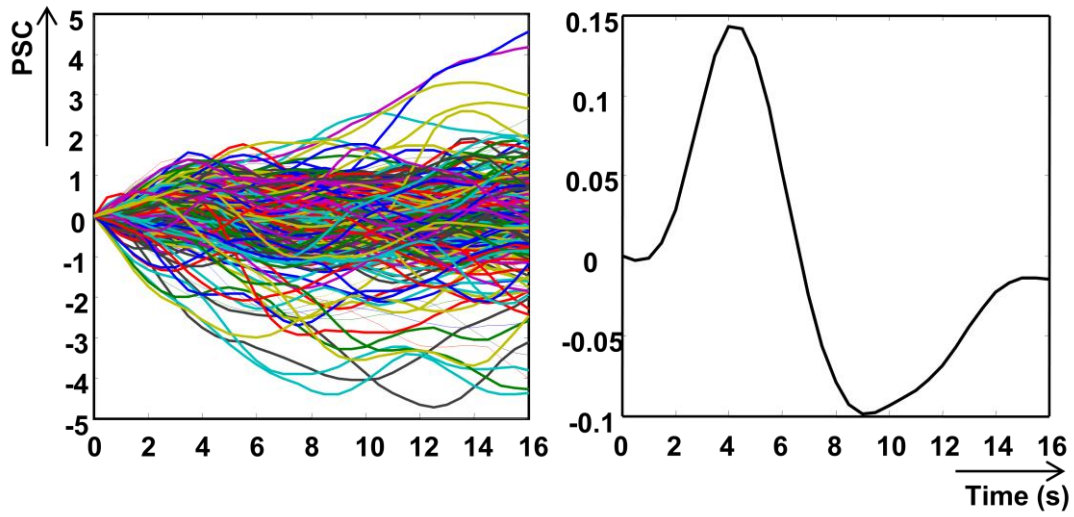

Figure 3.14: All the single trials from the auditory cortex (left panel) and the ensemble-averaged HRF from AC (right panel).

A second data set, the so-called 'non-active' (NA) one, was obtained in a similar manner using data from the fusiform gyrus in the occipital cortex (Figure 3.15 left panel). The total number of voxels in this region was 430, which is comparable with AC. The occipital cortex (OC) was selected because we used an auditory activation experiment which did not involve any visual stimulation, so we do not expect to find activity related to the presentation of auditory stimuli. The same number of trials was obtained from the OC as for the AC, and the ensemble-averaged signal is shown in Figure 3.15 (right panel). This figure confirms the absence of a meaningful response.

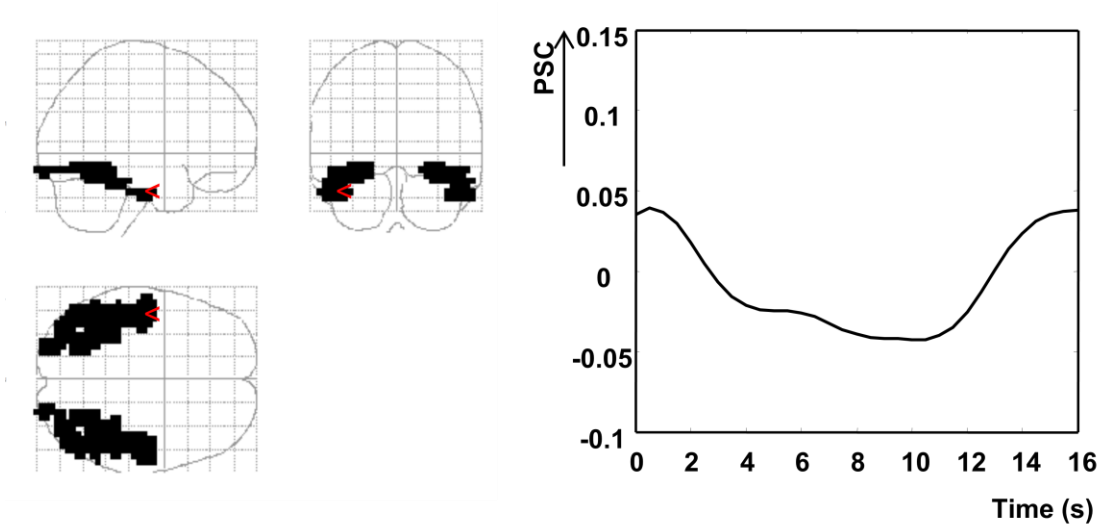

Figure 3.15: Spatial location of the occipital cortex (OC) (left panel) and the ensemble averaged HRF obtained from the OC (right panel).

Both datasets were analyzed using the correlation procedure with the template shown in Figure 3.16. First of all, to quantify the difference between the 'active' dataset and 'non-active' dataset, the histograms of the correlation coefficient between the averaged HRF across all trials in AC and each single trial in both groups of datasets were generated. The number of bins was set equal to the square root of the number of data points in the sample.

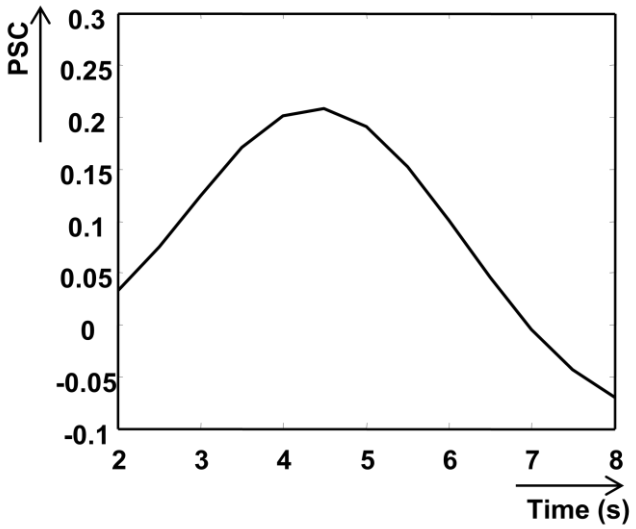

Figure 3.16: Ensemble-averaged windowed HRF across all trials in AC.

Figure 3.17 (a) shows the histogram of the correlation coefficients between the averaged HRF in AC and all the single trials in AC. Figure 3.17 (b) shows the same for the OC. The histogram shown in Figure 3.17 (b) appears uniformly distributed while the histogram in panel (a) is skewed towards larger, positive correlations. Theoretically speaking, when we select 0.5 as correlation coefficient threshold, the number of trials that are classified as activate should be close to 25% in OC, and above 25% in AC based on the histogram.

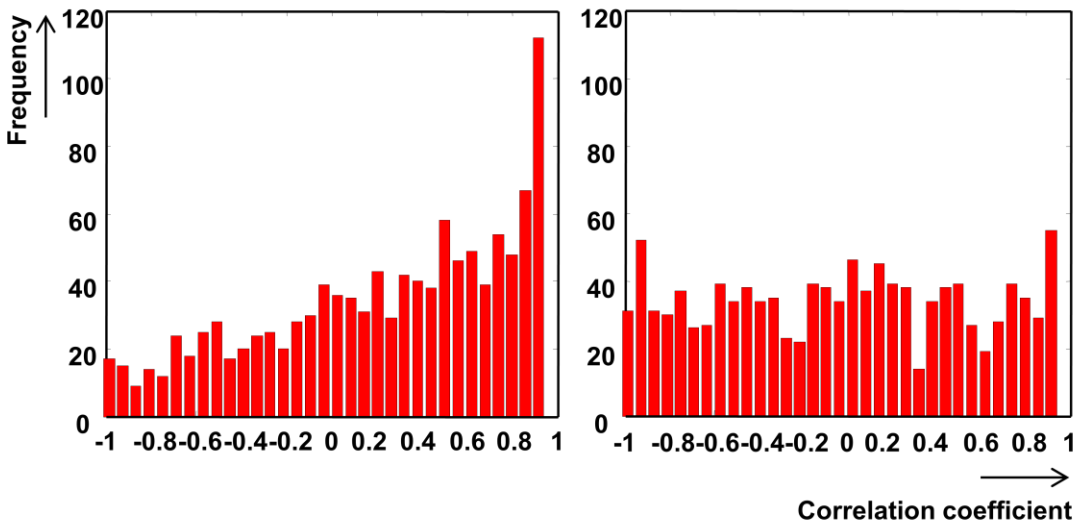

Figure 3.17: (a) Histogram of correlation coefficient between template and each single trial in the auditory cortex. (b) Histogram of correlation coefficient between template and each single trials in the visual cortex.

The scatter plot was used to assess the distribution of the values for both criteria. The scattergrams showing the correlation coefficient versus STD for all single trials in AC and OC are presented in Figure 3.18 and 3.19, respectively. It appears that STD spans a much larger range in AC than OC.

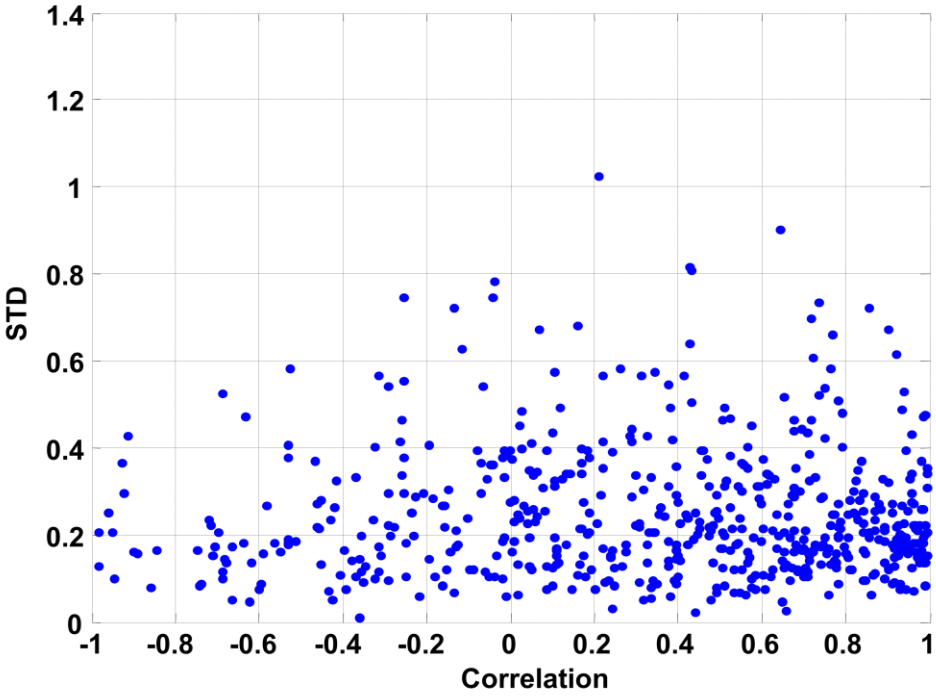

Figure 3.18: Scatter plot (correlation versus STD) of all single trials for AC.

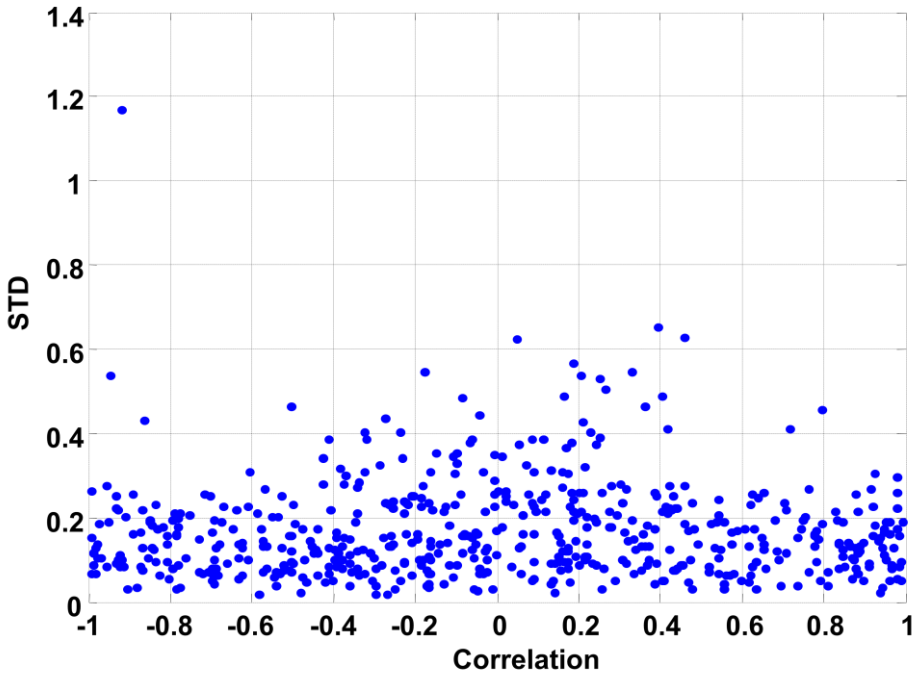

Figure 3.19: Scatter plot (correlation versus STD) of all single trials for OC.

Next, the single trials were classified using the ensemble average of all single trials from AC as template (Figure 3.16). A cross-correlation threshold of 0.4 and 2 times of the STD of the template was used in this test.

The number of active trials in AC was 278 and 288 trials were designated as inactive. The left panels in Figure 3.20 and 3.21 show all the active trials and all the non-active trials obtained from AC, respectively. The right panels in Figure 3.20 and 3.21 show the ensemble average of all the active trials and the ensemble average of all the non-active trials obtained from AC, respectively. The active trials showed a clear peak around 4 s, and the ensemble average of all active trials resembled the canonical HRF. On the other hand, the ensemble average of non-active trials did not show a response.

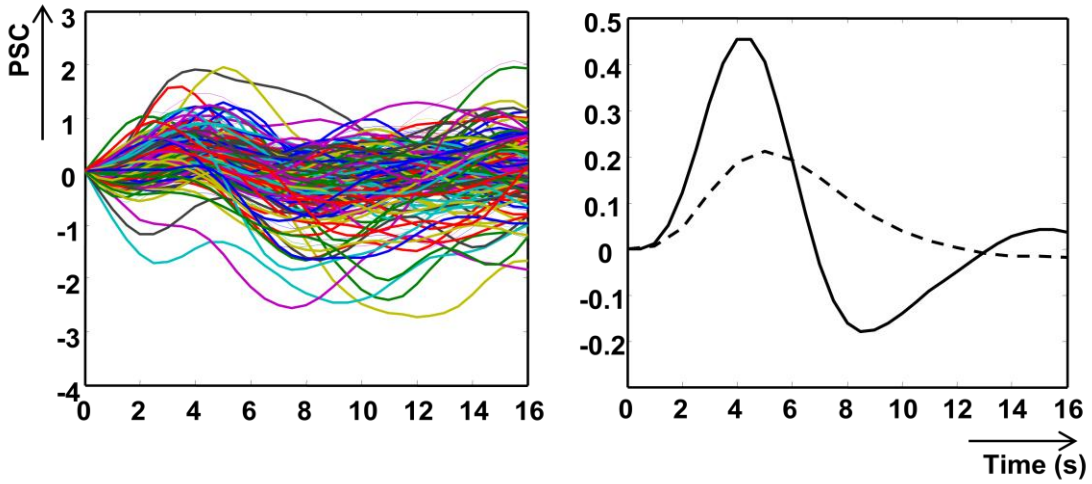

Figure 3.20: All active trials from AC (left panel) and the ensemble average HRF of all active trials from AC (solid line) with the canonical HRF (dash line) (right panel).

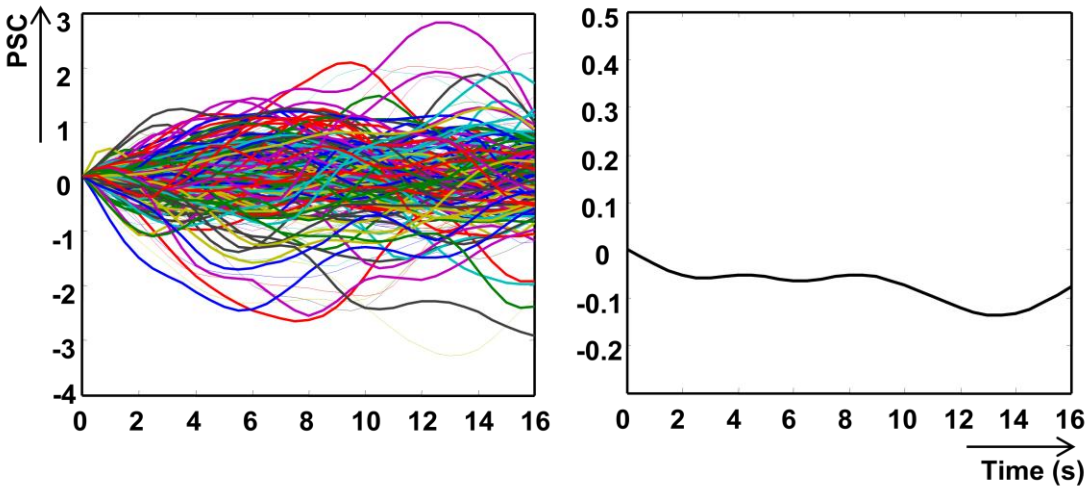

Figure 3.21: All non-active trials from AC (left panel) and ensemble averaged HRF of all non-active trials from AC (right panel).

The number of active trials in OC was 88 with 478 inactive trials. The left panels in Figure 3.22 and 3.23 show all the active trials and all the non-active trials obtained from OC, respectively. The right panels in Figure 3.22 and 3.23 show the ensemble average of all the active trials and the ensemble average of all the non-active trials obtained from OC, respectively. Note that a response can be seen in Figure 3.22 (right panel), and that it is only slightly smaller than the response seen over the AC (Figure 3.20 right panel). This shows a weakness of our correlation-based method. This weakness is not unexpected, as even random, band-pass filtered time series will occasionally show a correlation with a template. However, as long as the number of such trials will be small (or least much smaller than genuinely active trials), there is really no problem. Also, the ensemble average of non-active trials did not show a response. This result further confirms that the correlation-based method can successfully find distinct active and non-active clusters. We further compared the number of active trials in AC and OC.

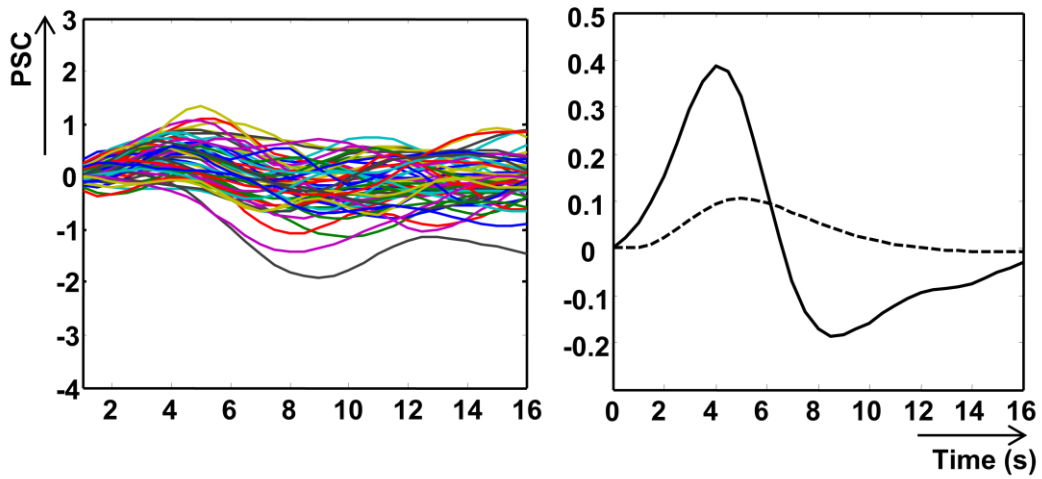

Figure 3.22: All active trials from OC (left panel) and the ensemble averaged HRF of all active trials from OC (solid line) with the canonical HRF (dash line) (right panel).

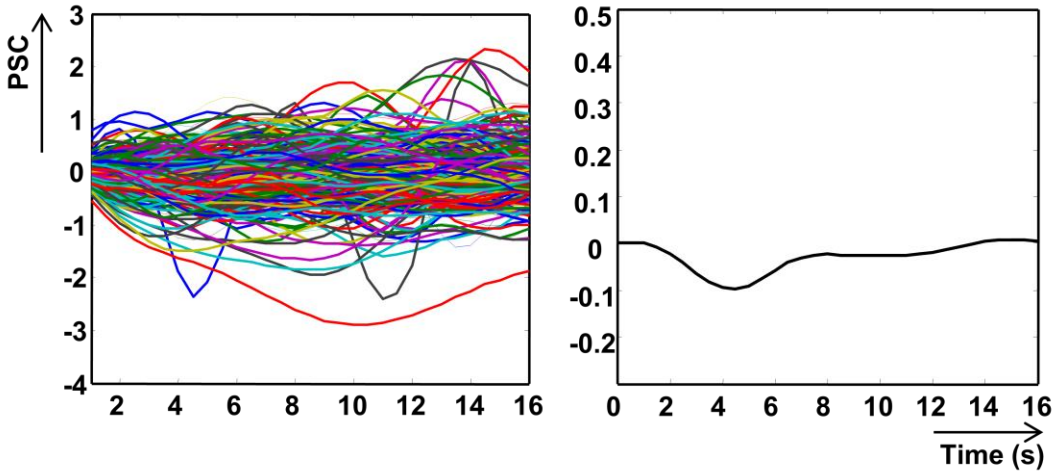

Figure 3.23: All non-active trials from OC (left panel) and the ensemble averaged HRF of all non-active trials from OC (right panel).

Table 3.3 presents the results of number of activated trials in AC and OC for each subject. It can be seen that the number of activated trials in AC was larger than the number of activated trials in OC. Two-sided *t*-test showed that the difference reached significance at threshold 0.4 (t=7.4, p<0.05,

df=13,). These results prove that AC produces more active responses than OC.

Table 3.3: Number of activated trials assigned to AC and OC for each subject and the *p* value, *t* value and degrees of freedom for comparing the number of activated trials between AC and OC at correlation threshold 0.4.

Sub	AC	OC
1	25	10
2	12	4
3	17	13
4	31	5
5	15	8
6	10	5
7	17	9
8	25	7
9	15	5
10	18	9
11	24	11
12	23	7
13	27	9
14	19	8
t	7.4	
p	<0.0001	
df	13	

In conclusion, the ‘active’ dataset produced more active responses than the ‘non-active’ dataset, showing that the correlation method can find significant difference between ROIs.

3.3.2 Comparison between different conditions

Next we determined the sensitivity of the cluster-based method by analyzing a different paradigm (e.g., listening to single tones or listening to double tones). Specifically, we expect that the auditory cortex produces more activation in response to double tones than single tones, and we will seek to confirm this with the clustering method.

The signal selection procedure is the same as chapter 3.3.1. The responses to *single* tones were the same as used in Section 3.3.1 (566 responses). The dataset for *double* tone response was obtained from the statistic map shown in Figure 3.24 (left panel). The statistical maps were thresholded at a p = 0.001 and any voxels within the ROI that exceeded this threshold were identified. This resulted in 447 voxels as being identified to make up the STG (left and right combined). The average time-series from the ROI was obtained and a DCT with cut-off frequency of 0.03 Hz was used to remove low-frequency noise. In all, 546 responses to double tones were obtained from 14 subjects. Finally, all trials were normalized to percentage signal change. Figure 3.24 (right panel) is the average signal of all trials for the double stimuli. Using the right panel of Figure 3.24 as template, the correlation coefficient and STD were computed and the scattergram is presented in Figure 3.25, which can be compared with Figure 3.18.

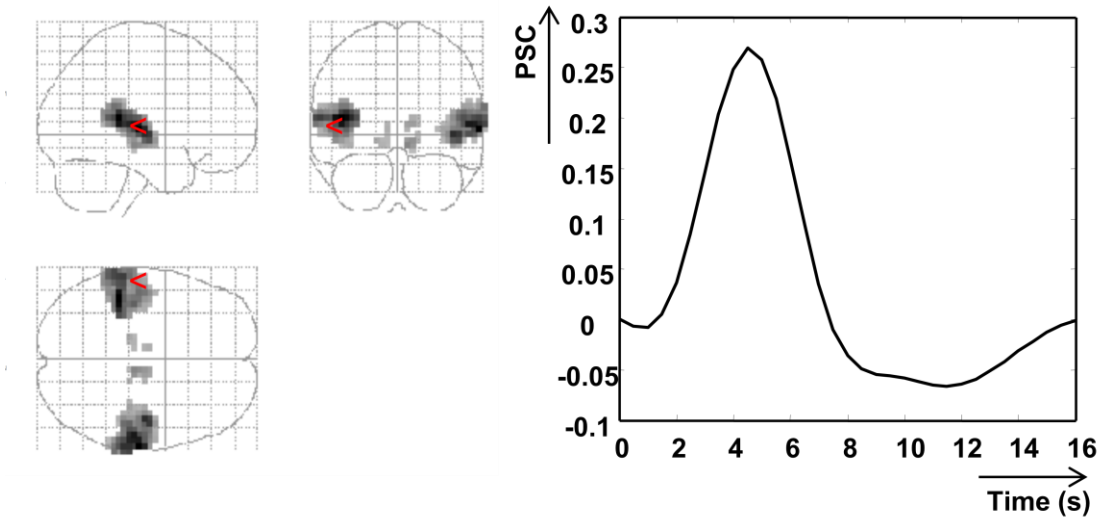

Figure 3.24: Statistical maps of AC for double stimuli at *p*<0.001 (left panel) and the averaged HRF from AC for double stimuli (right panel).

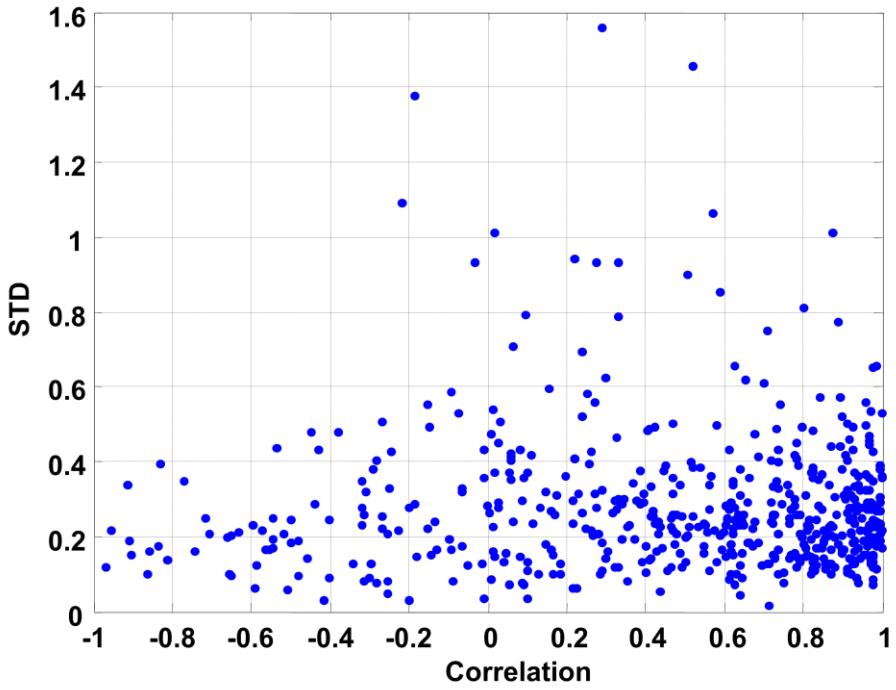

Figure 3.25: Scatter plot for single trial responses to double stimuli

Comparing Figure 3.18 and Figure 3.25, is appears that the difference between the double and single condition is much less than the difference between AC and OC. Both the single and double condition produced a more dense distribution toward the positive end of the correlation coefficient, but the double stimuli appeared to have more responses with a higher correlation coefficient than the single stimuli. There was no obvious difference between the two paradigms for the STD distribution.

To test the hypothesis that the different paradigms produced different activity patterns and that double stimuli are more active than the single stimuli, we compared the active clusters obtained from the ‘single’ dataset and ‘double’ dataset. For example, Figure 3.26 presents the active trials for the single and double stimulus paradigm using correlation threshold 0.4. The number of active trials for single stimuli was 278 (49.11%) and the number of active trials for double stimuli was 341 (60.24%). The ratio of the number of active trials for the double versus the single paradigm was 1.23.

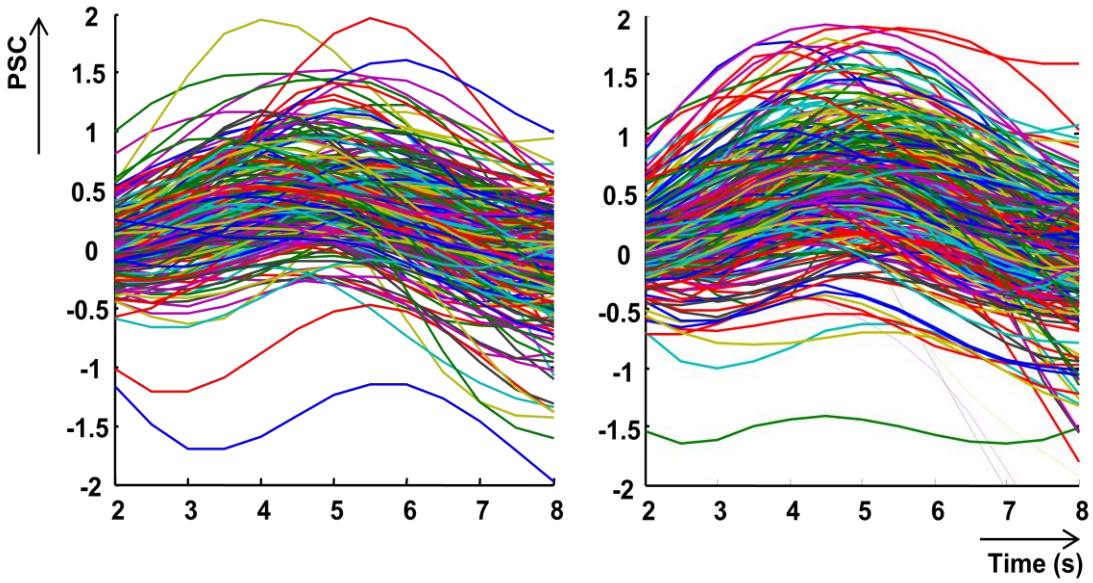

Figure 3.26: Active trials for single stimuli (left) and double stimuli (right) at threshold 0.4

Table 3.4 presents the number of active trials for the single stimuli dataset and the double stimuli for each subject at threshold 0.4. Two-sided *t*-test showed that the double stimulus paradigm produced significant more active trials than the single stimulus paradigm (t=3.44, p<0.05, df=13).

Table 3.4: Number of active trials for single and double stimuli for each subject, the *t* values, *p* values, and the degrees of freedom for comparing the number of active trials between single and double stimuli at correlation threshold 0.4.

sub	D	S
1	30	25
2	14	12
3	32	17
4	26	31
5	31	15
6	17	10
7	23	17
8	21	25
9	20	15
10	19	18
11	29	24
12	27	23
13	28	27
14	24	19
mean	24.36	17.64
t		3.44
p		0.004
df		13

The results show that 12 out of 14 subjects produced more active trials for double stimuli than single stimuli in STG, and the group difference reached a significant level. This result suggests that the correlation-based method can also be used to quantitatively distinguish the difference between two conditions.

Chapter 4: Comparison between conventional fMRI analysis and correlation-based analysis

4.1 Introduction

The focus of this chapter is to determine if the cluster-based method can improve conventional fMRI analysis. This will be achieved by exploring the brain regions responded to single stimuli using conventional fMRI analysis, using data collected from healthy subjects listening to single tones and paired tones. The same data will be analyzed using the cluster-based method and the results will be compared. We expect that by focusing on 'active' trials only, as determined by the clustering method, we will obtain better statistical maps and that the sensitivity of the fMRI data analysis will be increased through the identification of activated areas with a low signal-to-noise ratio.

Secondary objectives will be to determine if a BOLD signal due to auditory stimuli can be robustly measured or not in the noisy MRI scanner using the conventional EPI sequence; which regions are involved in processing single and double stimuli; and which regions are involved in sensory gating in healthy subjects.

4.2 Event-related fMRI experiment

4.2.1 Data acquisition

Fourteen healthy (5 female, 9 male) subjects participated in the fMRI experiments. The average age of the subjects was 24.6 years with a range of 20 years to 32 years. The standard deviation of the age distribution was 3 years. Each subject was interviewed before the scans, and had no self-reported history of neurological disease, major psychiatric disturbance, substance abuse, or psychoactive prescriptive medication usage.

4.2.2 Auditory stimulation paradigm

The study participants listened to auditory tones delivered through (air-driven) ear phones to both ears simultaneously while the subjects were in 3.0T research-dedicated, head-only Allegra Siemens fMRI scanners in the Human Neuro-Imaging Laboratory at Baylor College of Medicine. No behavioral responses were needed. The paradigm consisted of 80 randomized single or paired tones of 1000 Hz (4 ms in duration with a 2 ms rise and fall time, 0.5 s between tones in a pair); the average number of single and paired tones was maintained equal. The time between any two consequent events (single tone or pair of tones) was randomly chosen to be 16, 16.5, 17, 17.5, or 18 s which allows for the complete recovery of the HRF (Figure 4.1). The interval of at least 16s between events guarantees that the BOLD responses will have returned to baseline before the next stimulus is presented. A mixed paradigm (singles and pairs mixed randomly) ensures the comparability of certain uncontrollable factors such as attention fluctuations

and habituation for the two types of stimulus. The sound was adjusted to a high level to ensure that subjects were able to hear the stimulus clearly before the beginning of the scanning session and all subjects were instructed to report troubles with hearing the stimulus immediately to the experimenter by squeezing an emergency squeeze bulb provided to them beforehand.

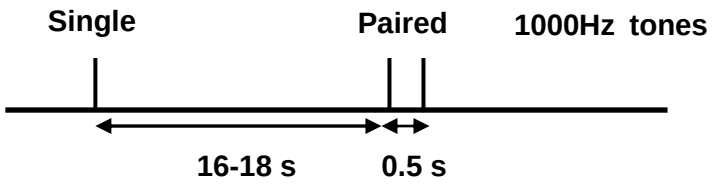

Figure 4.1: Auditory stimulation paradigm

4.2.3 MR imaging

High resolution T1-weighted 3-D anatomical scans were acquired for each subject using an MP-RAGE sequence (Siemens). Then continuous whole brain imaging was performed on the participants. Structural run details were as follows: fast spoiled gradient echo pulse sequence, 192 transversal slices, repetition time (TR) of 1200mm and echo time (TE) of 2.93ms; 256 x 208 matrix. Functional run details were as follows: echo-planar imaging, gradient recalled echo with 26 transversal slices, a repetition time (TR) of 2000ms and echo time (TE) of 40ms; flip angle=90°; 64x64 matrix, 4mm thick axial slices acquired parallel to the anterior/posterior commissural line for measurement of the BOLD effect. This yielded functional 3.3 mm x 3.3 mm x 4.0 mm voxels. Head motion was minimized with a head-conforming vacuum cushion.

4.2.4 FMRI data analysis

The fMRI data was analyzed using SPM2 (Welcome Dept. of Imaging Neuroscience, London). Data from each subject was realigned to the first volume using a six-parameter rigid body transformation within subjects to correct for subject movement. The average motion-corrected images were co-registered to each individual's structural image using a 12 parameter affine transformation. Slice timing artifacts were corrected depending on scan parameters and the images were spatially normalized to the Montreal Neurological Institute (MNI) template by applying a 12 parameter affine transformation, followed by a nonlinear warping using basis functions. The images were also re-sampled to 4 mm x 4 mm x 4 mm voxels during normalization. The images were smoothed with an 8 mm isotropic Gaussian kernel and a 128 s high pass filter was applied to remove low-frequency fluctuation in the BOLD signal.

The general linear model (GLM) was applied to estimate first-level measures identifying the effects of condition for each subject which can be used to determine what brain areas were involved in processing single tones and paired tones. Data were modeled with the canonical HRF included in SPM2.

A second level analysis - random effects was implemented using the one-sample t-test function to evaluate between subjects effect. Functional results were overlaid onto the group-averaged T1-weighted anatomical images for visualization and threshold at $p \leq 0.01$, uncorrected and minimum cluster size of 5 voxels. The p threshold was selected to be consistent with

other auditory sensory gating studies for the purpose of comparison. (Tregellas et al., 2007)

Masks were used to obtain the regions of interest (ROI). Masks are 3D image sets in which voxels belonging to a ROI have an intensity of one and background voxels an intensity of zero. One mask image was created per ROI. The mask and statistical parametric map produced using the canonical HRF were superimposed. Then the time series were extracted from the voxels in the corresponding ROIs and averaged across those voxels. Linear detrending was used to remove low-frequency trends introduced by unavoidable factors like scanner drift and physiological processes. Then, time series were interpolated by a factor of 4 to obtain a 500 ms interval. Single trial HRFs were obtained by using the stimuli time function. The single trials were normalized to percentage signal change and adjusted to set the value of the first point to zero for display purposes. All analyses were conducted in Matlab.

4.3 Results

4.3.1 Conventional fMRI analysis

4.3.1.1 Determine if a BOLD signal can be measured or not

First we determined if a BOLD signal due to auditory stimuli can be robustly measured in the noisy MRI scanner using the conventional EPI sequence. A fundamental problem of using fMRI to examine auditory system is the interference of the scanner's acoustic noise caused by the gradient switching of conventional echo-planar fMRI sequences with the experimental

stimulus. In the relatively few auditory fMRI studies of sensory gating, special procedures were designed to avoid the stimulus and noise interaction. Tregellas et al. (2007) used the clustered volume acquisition technique, which applied a silent period in the middle of an acquisition period. This technique requires a longer acquisition time than the conventional technique. Also, the temporal sampling rate will decrease dramatically and this will decrease the temporal resolution of HRF as well. A continuous EPI sequence that emits continuous noise rather than pulsed noise was used in Mayer et al. (2009). Compared to conventional fMRI, continuous fMRI reduced auditory cortex BOLD baseline and produced stronger responses with pure tones (Seifritz et al., 2006). Here we test whether a BOLD signal can be detected using conventional fMRI EPI sequences.

At the group level, the activation map for single stimuli was computed using random effects analyses. Results demonstrated that single stimuli consistently activated several regions (STG, THA, IFG and DLPFC) across the healthy subjects as shown in Figure 4.2. In particular, there were a significant numbers of voxels involved in the activation of STG.

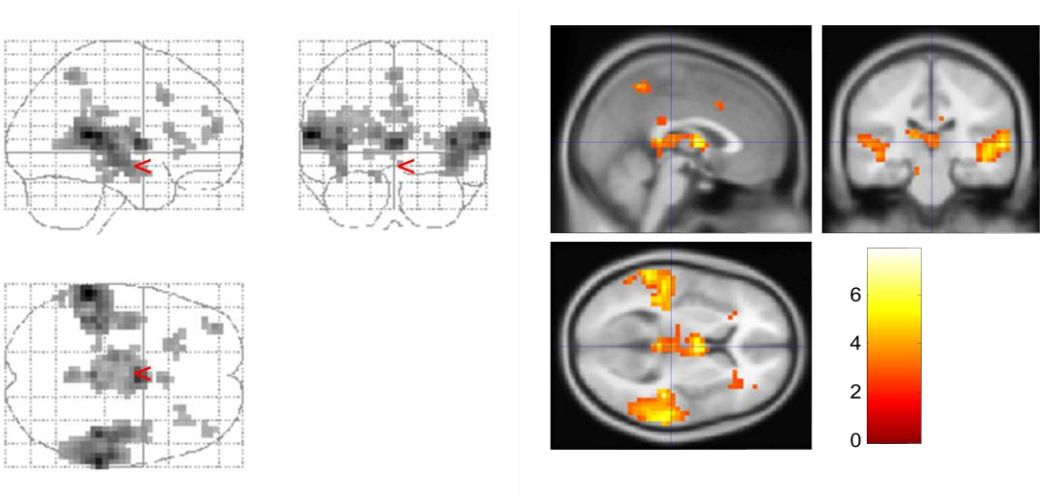

Figure 4.2: *p*<0.01, group (healthy controls) level statistical parametric map for single stimuli.

Table 4.1: Areas that demonstrated activation due to single stimuli (coordinates represent the most significant voxel in each cluster. *p*<0.01).

Region	Side	Coordinate X, Y, Z			Cluster size (no. voxels)	Z score	T value
STG	R	64	-32	12	317	4.43	6.98
STG	L	-60	-40	12	292	4.7	7.9
THA	R	4	-4	8	23	3.87	5.65
THA	L	-12	-20	12	43	3.47	4.7
IFG	R	35	32	4	13	2.5	2.89
IFG	L	-36	52	16	13	3.13	3.92
DLPFC	R	44	48	16	10	2.62	3.09
DLPFC	L	-36	52	16	13	3.13	3.92

To test whether robust responses to pure tones can be measured, two mask images were created: STGR and STGL, representing the right and left STG, respectively. The time series were extracted from the voxels in each ROI, and spatially averaged for each subject. The averaged power spectra of the time series within the STGR and STGL for 14 subjects were also

calculated and are presented in Figure 4.3. The peak of the spectra (0.0625 Hz) matches the frequency of the stimulus delivery (randomly chosen from 16, 16.5, 17, 17.5, or 18 s).

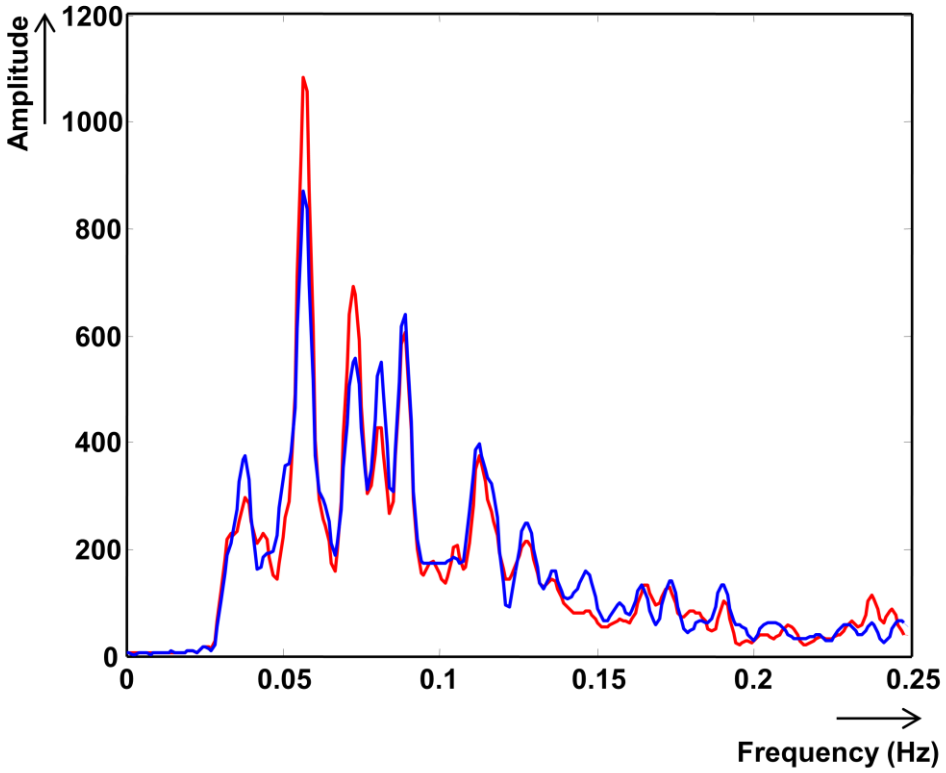

Figure 4.3: Power spectrum of time series from STGL (blue) and STGR (red)

The fact that the power spectrum of the time series from STGL and STGR contained the frequency of stimulus delivery indicated that the activation of the voxels was in response to the stimuli. These results show that robust BOLD signals reflecting auditory processing can be obtained in the noisy MRI environment.

4.3.1.2 Regions involved in processing single and double stimuli using conventional EPI sequence

Several areas were found to exceed the significance threshold (p<0.01; 5 voxels) during both processing the single (Figure 4.2) and paired tones (Figure 4.4). Double stimuli consistently activated STG, THA and DLPFC across healthy subjects, with a large number of voxels involved in STG activation. The common area results showed good concordance of activation areas across conditions in the bilateral auditory cortex (superior temporal gyrus -STG- and the transverse temporal gyrus -TTG-), and thalamus (THA) (Figure 4.5). The auditory cortex represents the auditory stimuli processing station. The thalamus is believed to both process and relay sensory information to the auditory cortex (Steriade et al., 1988). Both single and double tones activated the dorsolateral prefrontal cortex (DLPFC). The DLPFC is roughly equivalent to Brodmann areas 9 and 46 and provides inhibitory modulation of the auditory cortex (Knight et al., 1989). Also, the single tones activated the bilateral Inferior Frontal Gyrus (IFG). The IFG includes Brodmann areas 44 and 45, also known as Broca's area. Its function is linked to speech production (Plaza et al., 2009). The left IFG has been shown by a number of fMRI studies to play an important role in semantic processing (Poldrack et al., 1999).

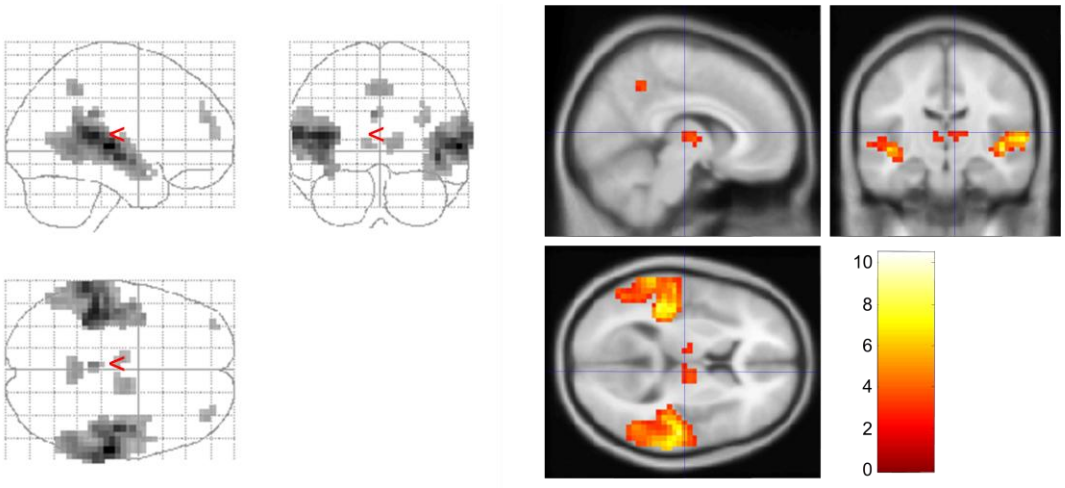

Figure 4.4: *p*<0.01, group level statistical map for double stimuli

Table 4.2: Areas that demonstrated activation due to double stimuli (coordinates represent the most significant voxel in each cluster. *p*<0.01)

Region	Side	Coordinate X, Y, Z			Cluster size (no. voxels)	Z score	T value
STG	R	60	-24	4	477	5.49	11.35
STG	L	-44	-32	12	422	5.14	9.63
THA	R	12	-6	4	23	3.14	4.03
THA	L	-8	-12	4	9	2.89	3.56
DLPFC	R	36	52	24	9	2.96	3.07
DLPFC	L	-36	56	12	5	2.57	3.05

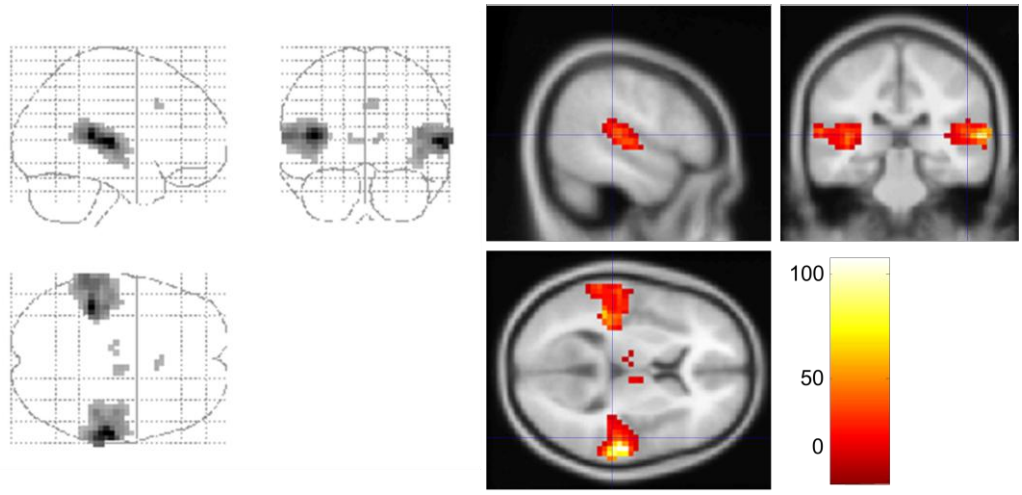

Figure 4.5: Group (healthy controls) level common statistical parametric map for single and double stimuli: *p*<0.01

Table 4.3: Areas that demonstrated activation due to single and double stimuli

Region	Side	Coordinate		X, Y, Z	Cluster size (no. voxels)	*z* score	*t* value
STG	R	64	-20	4	203	5.43	11.05
STG	L	-44	-36	12	239	5.43	11.03
THA	R	8	-24	-8	5	4.1	5.80
THA	L	-16	-28	-4	4	3.47	4.58

Several brain regions were found involving in processing single and double stimuli using conventional EPI sequence including STG, THA, IFG and DLPFC.

Worth notice, random and unknown systematic effects could lead to the differences in spatial location in response to single or double stimuli. For example, the location of DLPFC activation was slightly different for single and double stimuli. The common region may not reach the voxel threshold and

disappeared from the map. In this study, we separately selected the ROIs activation in response to single or double stimuli.

4.3.1.3 Brain regions involved in sensory gating using conventional analysis

One issue in examining sensory gating is the low temporal resolution (in the order of seconds) of fMRI technique. This makes it difficult to separate the response to the paired tone by only 500 ms which is used in traditional sensory gating paradigm. To address this issue, Mayer et al., (2009) empirically obtain HRF of paired tones (double tone) which was then compared to an estimated paired tone HRF. The estimated HRF for a double stimulus was obtained by interpolating and summing the HRF for the single-tone conditions to the same HRF delayed by 500 ms (single tone+single tone).

In healthy subjects, the electrophysiological response to a stimulus pair, as measured from the scalp is as shown in Figure 4.6. As one can see, the response to the second tone is smaller than for the first tone. We hypothesize that the corresponding HRF would follow the pattern shown in Figure 4.7 if gating happened. In other words, the HRF for S2 would be smaller than for S1. The total response, as obtained by fMRI, would then be the summation of the two responses. However, in the non-gating condition, the S2 response would be the same as S1, as shown in Figure 4.8 and the S1+S2 response in non-gating condition would be greater than the S1+S2 response in the gating condition. Therefore, we can use the Estimated HRF (as defined by Mayter et al.) as a control non-gating condition. We hypothesize that the magnitude of the Observed HRF would be smaller than the magnitude of Estimated HRF in the brain regions involving in sensory gating. We will use this technique to

examine the sensory gating network in healthy subjects. Specifically, the hypothesis was tested on the ROIs identified in 4.3.1.1 and 4.3.1.2 including the STG, IFG, DLPFC, and THA in healthy subjects.

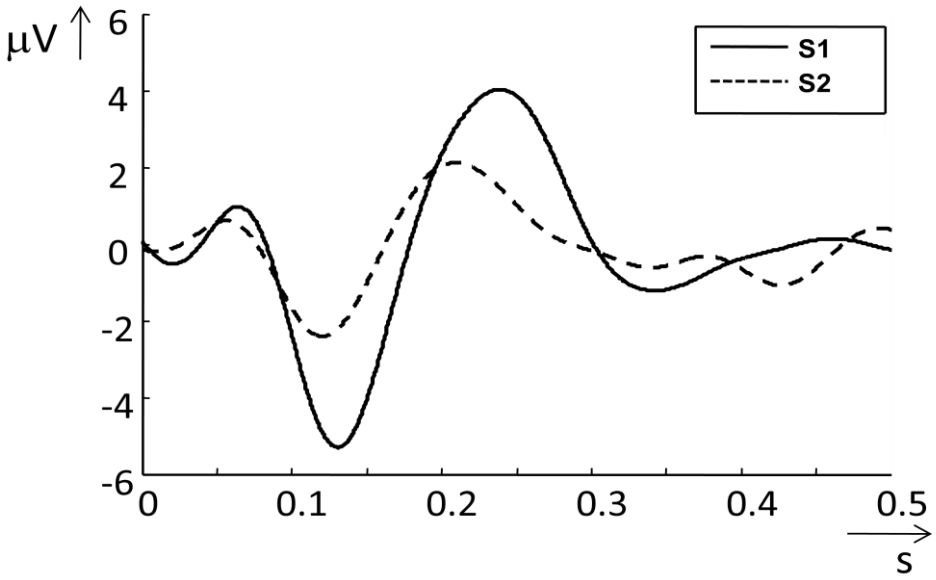

Figure 4.6: The underlying electrophysiological response for double tones in healthy subject. S1 response is the response to the first tone in a paired-tone. S2 response is the response to the second tone. S2 response is suppressed compared to S1 response in the normal gating condition.

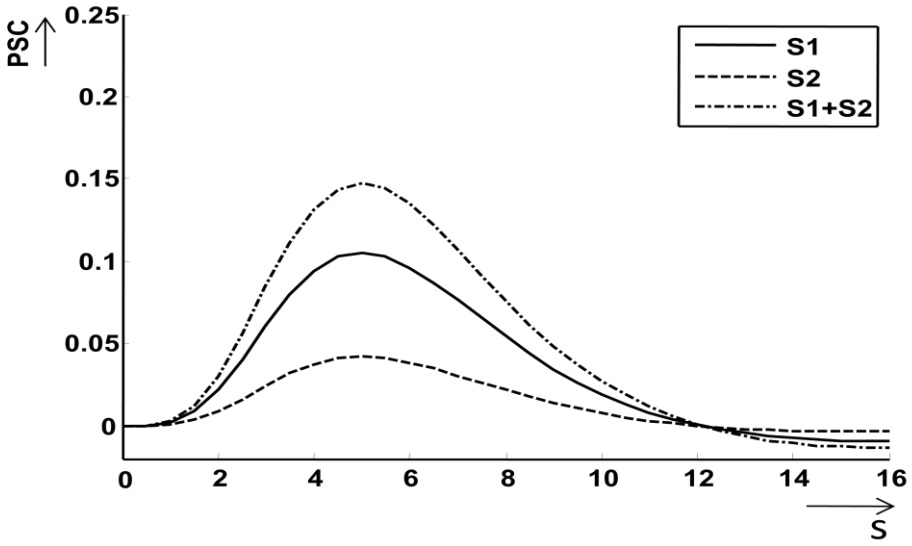

Figure 4.7: The gating condition. The HRFs are in percentage signal change (PSC) as a function of time (S). S1 is the theoretical HRF to the first tone in a paired-tone paradigm, and S2 is the theoretical HRF to the second tone. S1+S2 is the theoretical HRF for a paired-tone.

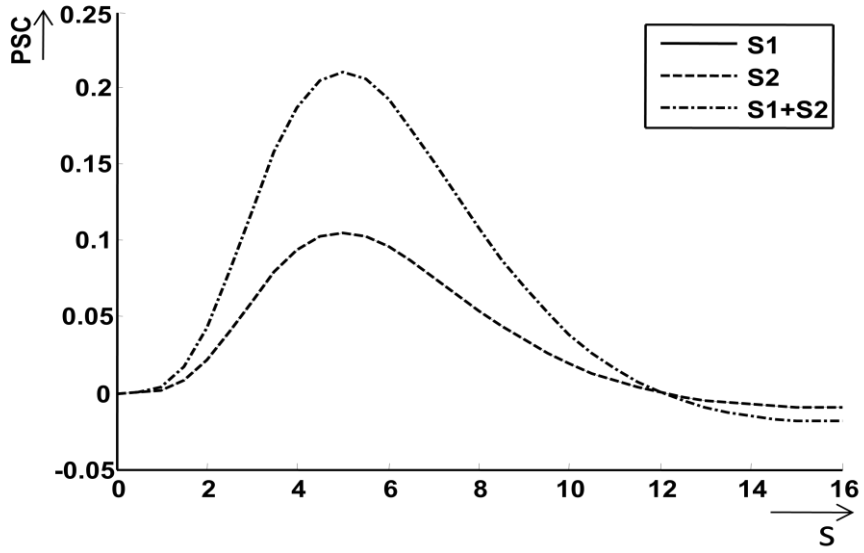

Figure 4.8: The non-gating condition. The HRFs are in percentage signal change (PSC) as a function of time (S). S1 is the theoretical HRF to the first tone in a paired-tone paradigm, and S2 is the theoretical HRF to the second tone. S1+S2 is the theoretical HRF for a paired-tone.

Figure 4.9 presents the grand averaged (across 14 subjects) of the Estimated HRF (blue curve) and the Observed HRF (red curve) obtained from 4 ROIs. Error bars represent the standard error. Two-sided *t*-test comparing the peak value of Estimated HRF and Observed HRF were done, *p* values were corrected for multiple comparisons using Bonferroni correction, and the results are presented in Table 4.4.

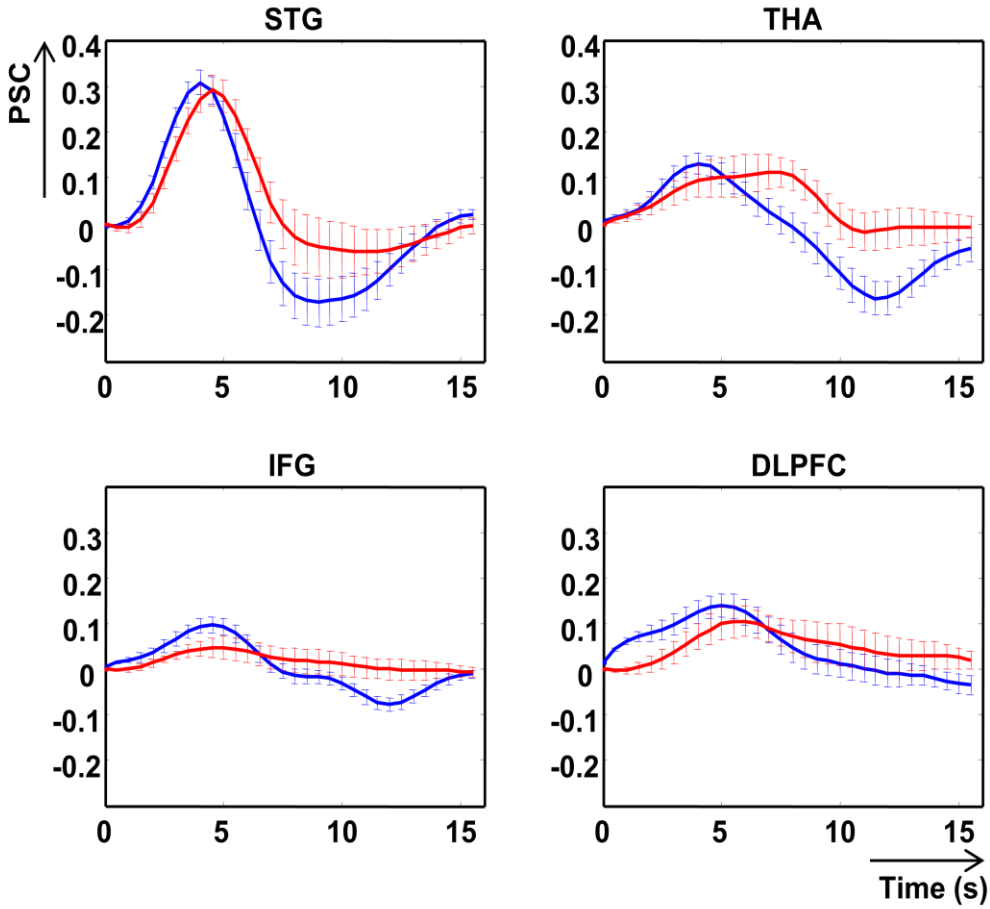

Figure 4.9: Estimated HRF (blue curve) and Observed HRF (red curve) for each ROI. Error bars represent standard deviations across the 14 sample subjects.

Table 4.4: Two sided *t* test for the peak value of the Estimated HRF and the Observed HRF for each ROI.

		STG	THA	IFG	DLPFC
Estimated HRF	mean	0.31	0.13	0.10	0.14
	sd	0.03	0.02	0.02	0.03
Observed HRF	mean	0.29	0.11	0.05	0.10
	sd	0.03	0.04	0.02	0.04
	t	0.39	0.41	1.83	0.80
	p	0.70	0.69	0.08	0.43

No significant difference between the Estimated HRFs and Observed HRF were found in any ROIs ($p>0.05$, Bonferroni correction was applied).

To our knowledge there have been no fMRI studies that investigated the hemispheric generators of sensory gating in the healthy subjects. In this follow up test, we examined the possible lateralized differences in the peak amplitude of Estimated HRFs and Observed HRF, and in the number of active trials for all four ROIs.

The lateralization analysis was carried out for the all ROIs STG, DLPFC, IFG and THA. Each ROI was further divided into a right side ROI and a left side ROI. The Estimated HRFs and the Observed HRFs are presented in Figure 4.10 for each ROI. The mean value, standard deviation and degree of freedom of the peak value of Estimated-HRF and Observed-HRF are presented in Table 4.5 and the two-sided *t*-test results are presented in Table 4.6, *p* values were corrected for multiple comparisons using Bonferroni correction.

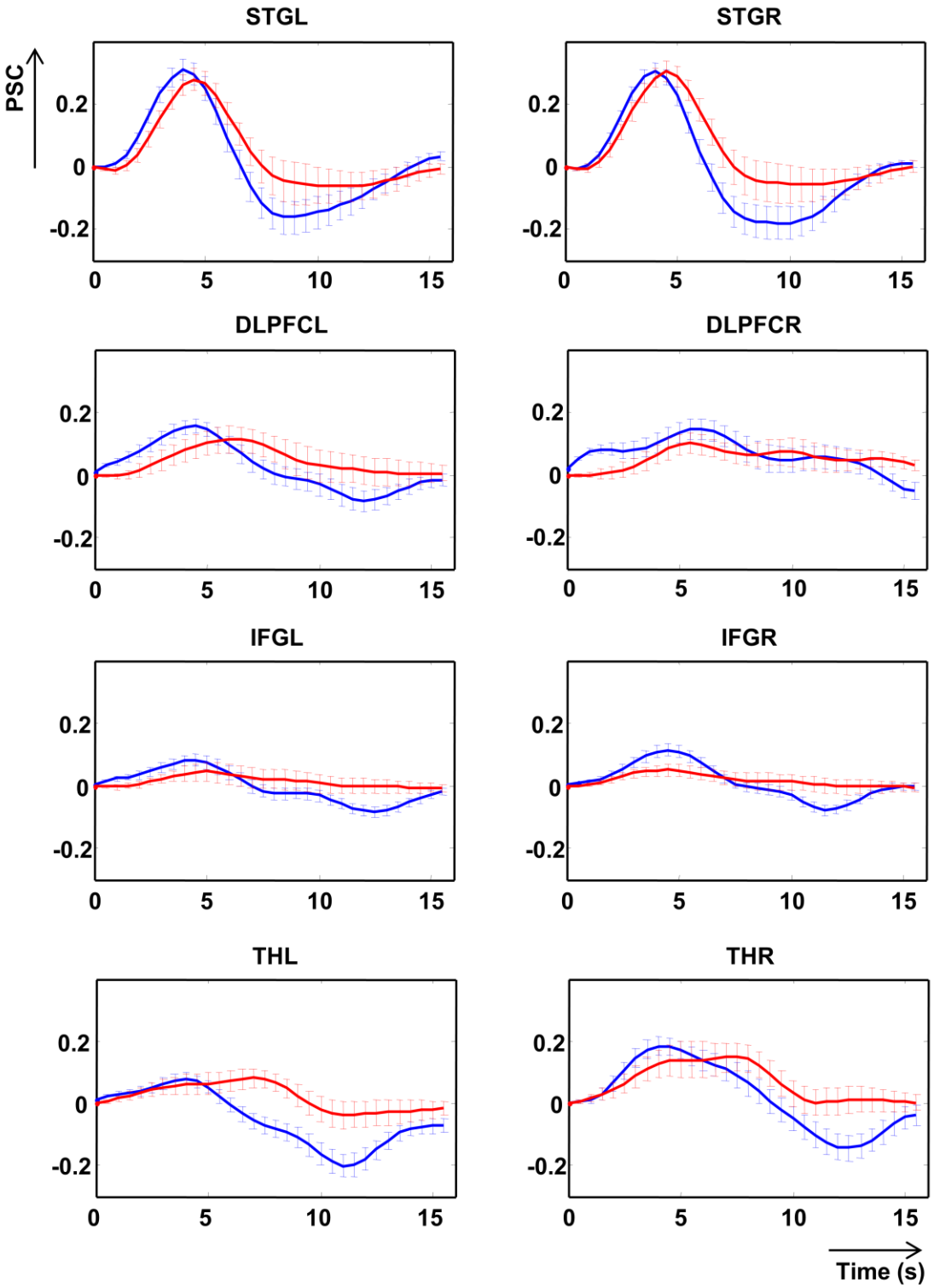

Figure 4.10: Estimated HRF (blue curve) and Observed HRF (red curve) for each ROI. Error bars represent standard deviations across the 14 sample subjects.

Table 4.5: The mean, standard deviation (sd) and degree of freedom (df) of peak value of the Estimated HRF (E) and the Observed HRF (O) for each left and right ROI.

		STG		DLPFC		IFG		THA	
		L	R	L	R	L	R	L	R
E	mean	0.31	0.31	0.16	0.15	0.08	0.11	0.08	0.18
	sd	0.03	0.02	0.02	0.03	0.02	0.02	0.02	0.03
O	mean	0.28	0.30	0.11	0.10	0.05	0.05	0.08	0.15
	sd	0.04	0.03	0.04	0.03	0.03	0.02	0.03	0.04
	df	13	13	13	13	13	13	13	13

Table 4.6: The *t* values and *p* values of peak value for comparing Estimated HRF (E) and the Observed HRF (O) for each left and right ROI.

		STG		DLPFC		IFG		THA	
		L	R	L	R	L	R	L	R
E vs. O	*t*	0.62	0.09	0.92	1.00	1.00	2.46	-0.08	0.68
	p	0.54	0.93	0.37	0.33	0.33	0.02	0.94	0.50

The results show that the Estimated HRFs were not significantly different (larger) than Observed HRFs in either the left or right side ROIs ($p>0.05$, Bonferroni correction applied) (Table 4.5 and Figure 4.10).

Two-sided *t*-test were also carried out to compare the difference of the peak value between the left and right hemisphere for both Estimated HRF and Observed HRF. *P* values were corrected for multiple comparisons using Bonferroni correction, and the results are presented in Table 4.7.

Table 4.7: *T* values and *p* values for comparing the peak value of the left and right hemisphere for both Estimated HRF (E) and Observed HRF (O).

		STG		DLPFC		IFG		THA	
		E	O	E	O	E	O	E	O
L vs. R	*t*	0.00	-0.40	0.28	0.20	-1.06	0.00	-2.77	-1.40
	p	1.00	0.69	0.78	0.84	0.30	1.00	0.01	0.17

Again, no significant difference was found between the left and right ROIs for both Estimated HRF and Observed HRF ($p>0.05$, Bonferroni correction applied).

In summary, we found that a conventional fMRI can be used to detect robust BOLD signal associated with auditory information processing. Brain areas involved in processing single and double stimuli included STG, DLPFC and THA. Previous evidence of STG, DLPFC and THA involvement in processing pure auditory tones has been reported by others (Tregellas et al., 2007; Mayer et al. 2009). The IFG involvement was also reported in Mayer's finding.

We were not able to determine which brain areas were involved in sensory gating. THA, DLPFC involvement in sensory gating has been suggested in prior fMRI studies of gating (Mayer et al., 2009; Tregellas et al., 2007). In addition, STG was reported to be involved in gating by Mayer et al. (2009). No IFG involvement in gating was reported in auditory fMRI studies.

In Chapter 5, we will conduct the same analysis using correlation-based method to determine if more conclusive information can be found.

4.3.2 Comparison between conventional fMRI analysis and correlation-based analysis

Here we tested whether the cluster-based method can improve upon conventional fMRI analysis by analyzing the same data using the cluster-based method and using conventional fMRI analysis and comparing the results.

The comparison was done in two stages. First, we determined if the cluster-based method resulted in HRF estimates that modeled the data better than the canonical HRF or the subject-specific HRF (ensemble averaged). Next, we compared the SPM results using the cluster-based approach and the conventional analysis.

In the following, we will use several HRF estimates. First, there is the canonical HRF (C-HRF). Second, there is the ensemble averaged, subject-specific HRF (ES-HRF). The ES-HRF is obtained by averaging all trials for a given subject and voxel (or ROI). The third average is the active, subject-specific HRF (AS-HRF) obtained by ensemble-averaging the *active* trials only for a given subject and voxel (or ROI).

4.3.2.1 Subject-specific HRF in healthy subjects

First, we recovered the ES-HRF and AS-HRF in STG for each subject. Time series from all voxels in the STG were extracted, and an averaged time series was computed for each subject over all voxels in the STG. All trials in response to single tones were used to characterize the subject-specific HRFs. The ES-HRF was obtained by averaging all trials for a given subject. The AS-

HRF was obtained using the correlation-based method with the ES-HRF as template. The ensemble average of the active trials served as AS-HRF. Based on the evaluation results presented in Chapter 3, the correlation threshold was set at 0.4 and standard deviation was set as two times the standard deviation of the template. As an example, Figure 4.11 shows all single trials for subject 1 (left) and the trials deemed active for the same subject (right). As expected, the right panel of Figure 4.11 shows that the active trials appear more consistent in the 2 s to 8 s interval than the unprocessed trials.

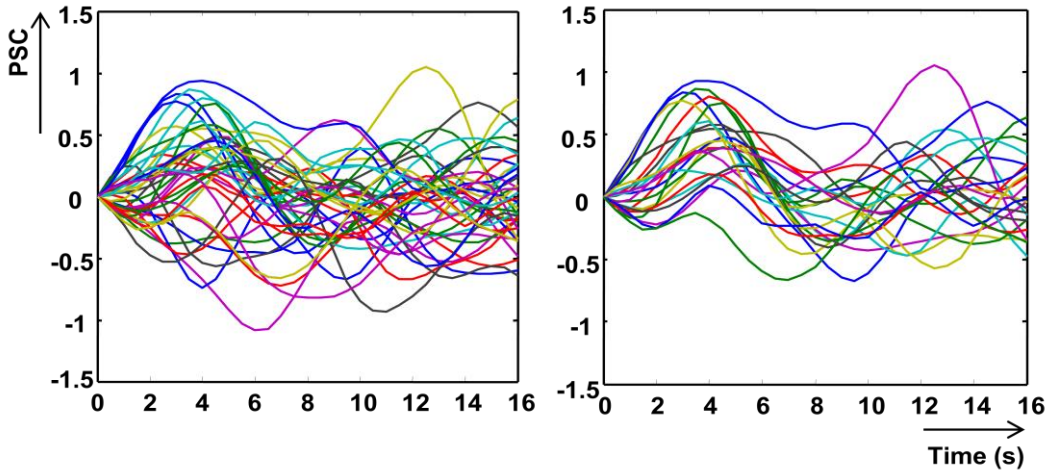

Figure 4.11: All trials from subject 1 (left), and the active trials for subject 1 (right) at threshold 0.4 and STD 0.4.

Figure 4.12 presents the C-HRF, ES-HRF and AS-HRF, respectively for each subject. The results indicate that the C-HRF, ES-HRF and AS-HRF have different time to peak. While the shapes are very similar before peak time, after peak time, the C-HRF used in SPM has a broader first peak, the subject-specific HRFs have deeper undershoots and the AS-HRF has higher amplitudes than the other two HRFs.

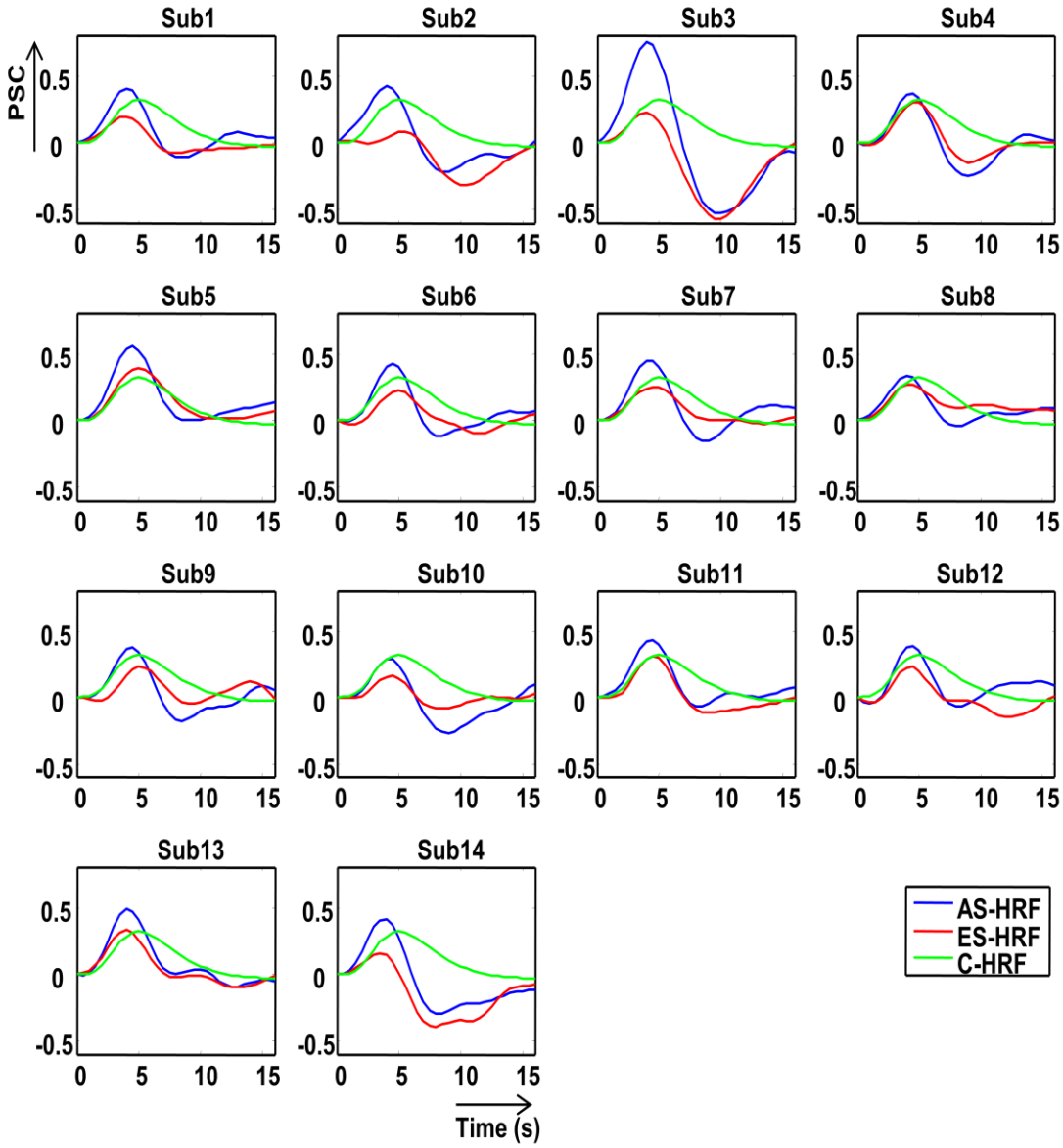

Figure 4.12: The ensemble-averaged subject-specific HRF (ES-HRF) for each healthy subject (red line), the active subject-specific HRF (AS-HRF) for each healthy subject (blue line) and the canonical HRF (C-HRF) (green line).

Across the subjects, the percentage signal change of the peak of ES-HRFs was 0.22% ± 0.1% (n=14, range 0.075% to 0.37%) and the mean time-to-peak value was 5 s ± 0.57 s (n=14, range: 4 s to 6 s).

The mean peak signal change of AS-HRF from baseline was 0.49% ± 0.18% (n=14, range 0.22% to 0.97%) and the mean time-to-peak value was 4.7 s ± 0.38 s (n=14, range: 4 s to 5.5 s).

The time-to-peak value of the canonical HRF was 5.5 s. The results show that the ES-HRFs and AS-HRFs have earlier time-to-peak than the C-HRF, and the time-to-peak ranges of the ES-HRFs were wider than the AS-HRFs.

The goodness of fit (*R*) for each type of HRF was determined using

$$R = SS_E \ / (n - p), \text{ with} \tag{4-1}$$

$$SS_E = \sum_{i=1}^{n} (y_i - \hat{y}_i)^2 , \tag{4-2}$$

where SS_E is the residual sum of squares, *n* is the number of observations and *p* is the number of explanatory variables used in the models. In equation 4-2, y_i is the i^{th} value of the BOLD signal and $\hat{y}_i$ is its predicted value. Roughly speaking, *R* is a measure of the discrepancy between the data and an estimation model. A small *R* indicates a tight fit between the model and the data. The HRF that has the smallest *R* is the best HRF. We expect to find significant differences between the AS-HRF and the other two HRFs, with the AS-HRF having the best fit and providing the smallest *R* among these three HRFs.

The *R* values for each HRF and each subject are shown in Table 4.8 and Figure 4.13. The results show that the AS-HRF's *R* values are the

smallest among the three. ES-HRF and C-HRF provide similar mean *R* value for all subjects (0.101 versus 0.105). Paired *t* test found a significant difference between the AS-HRF and ES-HRF (p = 0.007, t=2.84, df=13). The difference between the AS-HRF and C-HRF was also significant (p=0.006, t=2.92, df=13). However, no significant difference was found between ES-HRF and C-HRF (p=0.174, t=0.97, df=13). Thus, the AS-HRFs provide the best fit between the model and the data in all subjects.

It should be noted that subject 3 shows comparatively large *R* values indicating a great deal of discrepancy between the data and all of the three HRF models i. Examination of the activation map of subject 3 showed no activity in STG (at p<0.01), and the single trials displaying large variability, thus explaining the outlier status of this subject.

Table 4.8: The *R* values and the degree of freedom (df) for the AS-HRF, ES-HRF and C-HRF for each subjects.

	AS- HRF	ES-HRF	C-HRF
sub1	0.039	0.041	0.048
sub2	0.052	0.079	0.087
sub3	0.231	0.376	0.412
sub4	0.044	0.048	0.053
sub5	0.041	0.041	0.043
sub6	0.072	0.086	0.084
sub7	0.035	0.055	0.053
sub8	0.025	0.032	0.031
sub9	0.106	0.179	0.149
sub10	0.106	0.124	0.130
sub11	0.056	0.058	0.060
sub12	0.057	0.095	0.084
sub13	0.047	0.062	0.063
sub14	0.088	0.138	0.176
mean	0.071	0.101	0.105
df	13	13	13

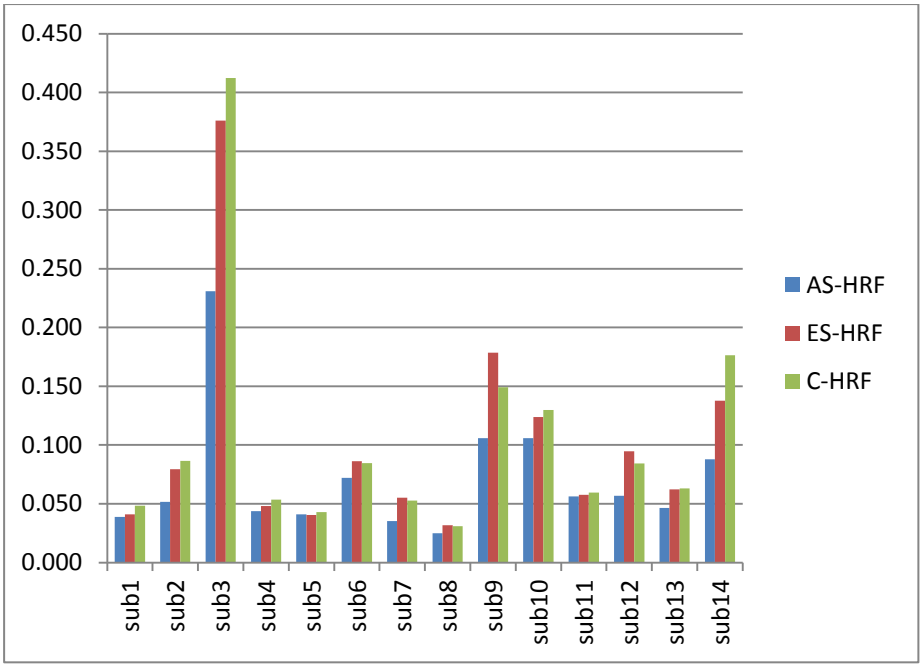

Figure 4.13: R value for AS-HRF, ES-HRF and C-HRF. The AS- HRF's R values are smallest among the three.

4.3.2.2 Comparing conventional versus correlation-based SPM

In this section, we investigated if using AS-HRFs rather than C-HRF increased detection sensitivity, and thus could delineate more precisely the activated areas.

First, we obtained an estimate of the AS-HRF in the AC for each healthy subject (see 4.3.2.1 and Figure 4.12). Second, the t-statistic maps were estimated using the AS-HRF and compared with regard to the activated areas and t-statistical scores obtained with a standard C-HRF. A standard anatomical mask of STG from WFU_pickatlas was used to count the active voxels in that region. The group level activity maps were obtained for the C-HRF (Figure 4.14) and AS-HRF (Figure 4.15).

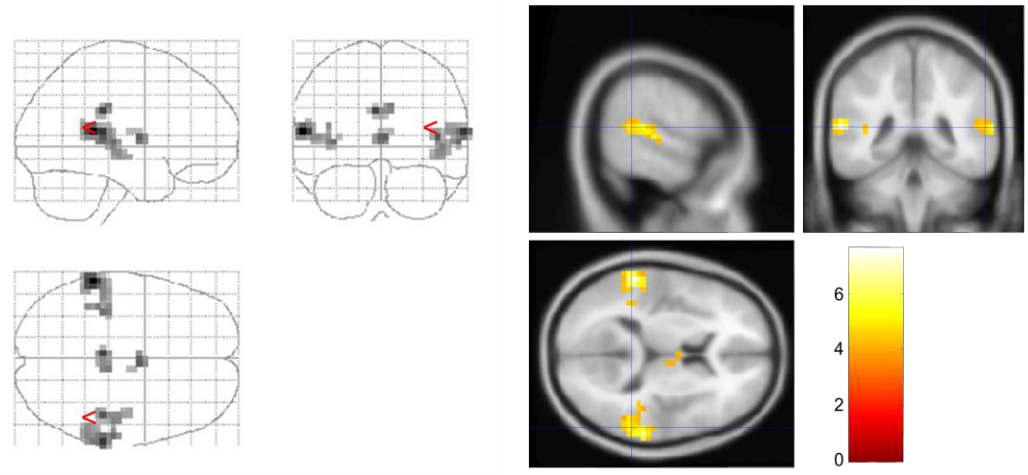

Figure 4.14: Group level statistical parametric map for single stimuli using C-HRF: $p < 0.001$

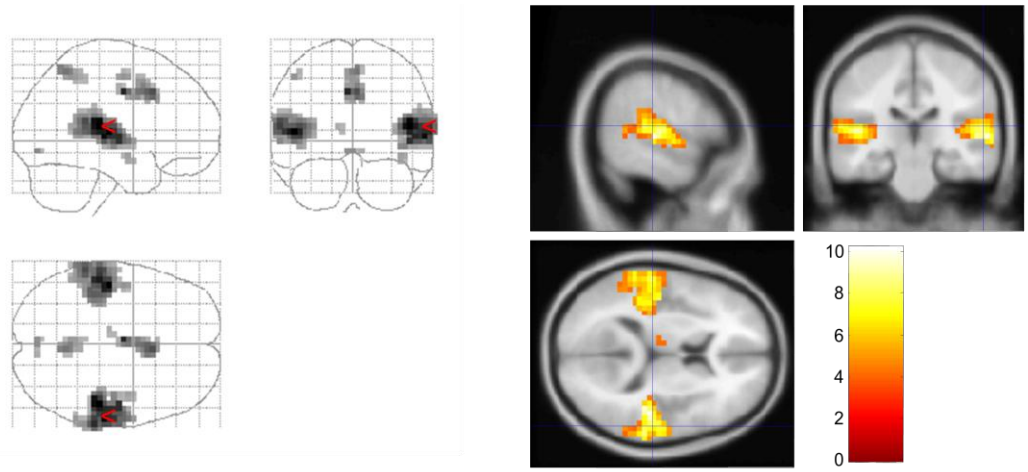

Figure 4.15: Group level statistical parametric map for single stimuli using AS-HRF: $p < 0.001$

We found that the use of AS-HRF increased sensitivity compared to the canonical HRF. Specifically, as shown in Table 4.9, the detection sensitivity, as judged by the average number of active voxels, increased by 58.2% in the AC ($p<0.002$), the mean *t* scores increased by 12% ($p<0.09$) and the maximum *t* scores increased by 15.9% ($p<0.07$).

Table 4.9: The activated number of voxels in STG, mean *t* scores and maximum *t* scores across active voxels obtained with the C-HRF (Top table) and the AS-HRFs (bottom table).

	C-HRF			AS- HRF		
Sub	# voxel	mean *t*	Max *t*	# voxel	mean *t*	Max *t*
1	102	3.3	5.73	189	3.5	6.26
2	145	3.54	6.86	205	3.5	6.33
3	0	0	0	169	3.5	5.47
4	290	3.77	7.64	381	4.5	9.92
5	422	4.73	9.64	425	4.9	9.62
6	52	2.7	4	22	2.5	2.8
7	109	3.4	5.3	102	3.3	6.1
8	152	3.1	5.7	256	3.6	7.3
9	100	3.14	4.86	145	3	4.98
10	130	3.9	8	115	3	4.7
11	150	4	7.4	230	3.8	7.9
12	100	3.3	6.2	219	3.9	6.7
13	117	3.5	5.5	212	3.8	8
14	4	2.5	2.5	298	3.4	5.9
mean	134	3.201	5.666	212	3.6	6.568

Figure 4.14 and 4.15 show that most of the voxels (93.33%) in the STG of the t-map using the C-HRF overlapped with the t-map using the AS-HRF (common activated voxels: 252, C-HRF activated voxels: 270, Subject-specific HRF activated voxels: 482). The AS-HRF detected larger activated regions. Worth noticing is that, subject 6, 7 and 10 showed a decreased number of active voxels. We further examined these three subjects and found their activation regions were toward the posterior of STG, and the standard anatomical mask only covered part of the activation regions. Even through the activation region increased by using the AS-HRF, we did not capture it by only counting the number of active voxels within the mask.

In summary, by removing the non-active trials, we obtained an increase in the volume of responses, and thus improved the SPM processing. One may argue that the AS-HRF improves on the C-HRF in two ways; the AS-HRF is subject-specific and it is based on active responses only. However, since we did not find a significant difference between the C-HRF and ES-HRF in terms of the goodness fitness of data, the increase in performance must be primarily due to the use of active trials.

Chapter 5: Acquiring new knowledge using the single-trial method

5.1 Introduction

In Chapter 4, we successfully identified the brain areas that are involved in auditory information processing using conventional fMRI analysis. However, the conventional method was not able to determine which areas are involved in sensory gating. Given that the correlation-based analysis is demonstrably more sensitive than the conventional analysis, we reanalyzed the data focusing on the active trials only. We also took advantage of the added analysis capabilities of the clustering method, such as measuring the number of active trials and the string-based approach (see Chapter 3) to further investigate the sensory gating network.

5.2 Methods

The data and auditory stimulation paradigm that were used in this experiment are the same as described in section 4.2.1 and 4.2.2, respectively.

Our results presented in Chapter 4 suggest the involvement of the superior temporal gyrus (STG), the bilateral inferior frontal gyrus (IFG), dorsolateral prefrontal cortex (DLPFC), and thalamus (THA) in auditory information processing and sensory gating in general. Therefore, these four ROIs were used to further investigate the difference in activity patterns between single and double stimuli paradigms.

First, we obtained the active trials for single and double stimuli for each ROI using the correlation-based method. The grand ensemble average of the active trials in response to double stimuli across all subjects was computed and is referred to as the Active-Observed HRFs. We also obtained the Active-Estimated HRFs for double stimuli by adding the average computed from the active trials in response to single stimuli across all subjects, to the same HRF delayed by 500 ms (single tone + single tone). The percentage of active trials for single and double stimuli for each ROI was also calculated. To investigate possible lateralization effects, each ROI was further divided into a right side and left side ROI.

Next, the string-based analysis was carried out on the ROIs. Each of the trials from a specific ROI was labeled as active (1) or non-active (0) using the clustering method with the template and threshold as used in 4.3.2.1. Combining the results across the ROIs, each trial was represented by a string of characters. These strings were searched to see if a particular pattern of active/non-active ROIs is more prevalent for the single tone experiments than the double tone experiments, thus providing insight into what activation patterns are characteristic for gating and which are not. The number of trials in each category (000 to 111) was also calculated.

5.3 Results

5.3.1 Brain regions involved in sensory gating

First, we obtained the region-specific templates for each single and double stimuli, by computing the grand average across all single and double stimulus responses, respectively, and the results are shown in Figure 5.1. It should be noted that the grand averages (across all 14 subjects) are rather small for all ROIs except for the STG.

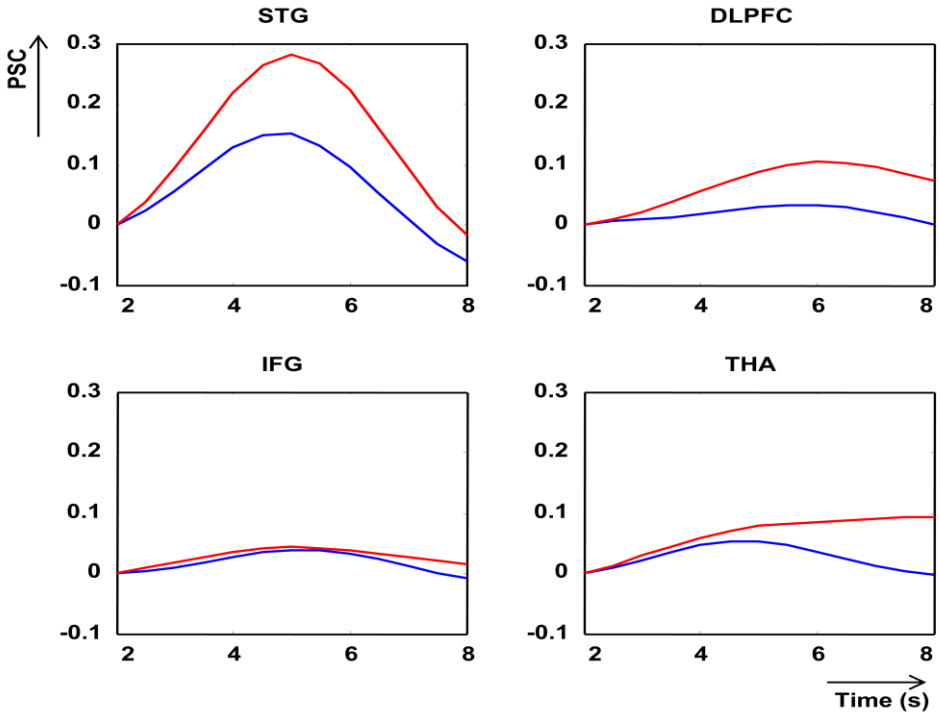

Figure 5.1: Templates for single (blue) and double (red) stimuli for each ROI.

Next, the active trials for each ROI and each stimulus paradigm were obtained using the corresponding templates, and the grand-averaged Active-Estimated HRF for the single and double stimuli were computed, respectively.

The results, presented in Figure 5.2, show that the peak latency for the THA response to double stimuli is delayed by several seconds compared to the single tone responses. This is physiologically unlikely and suggests a problem with the template matching technique. As we already observed before, the templates shown in Figure 5.1 are rather small (except for STG), and the double stimulus template for THA in particular does not show a clear peak but continues to increase to 8 s, whereas the single stimulus template has a peak at 5 s. As a result, the THA double-stimulus trials identified as active will peak much later than the single stimulus ones. To remedy this situation, it may be better to use the template as the ensemble average computed from the ROI with the most robust response, rather than ROI-specific templates.

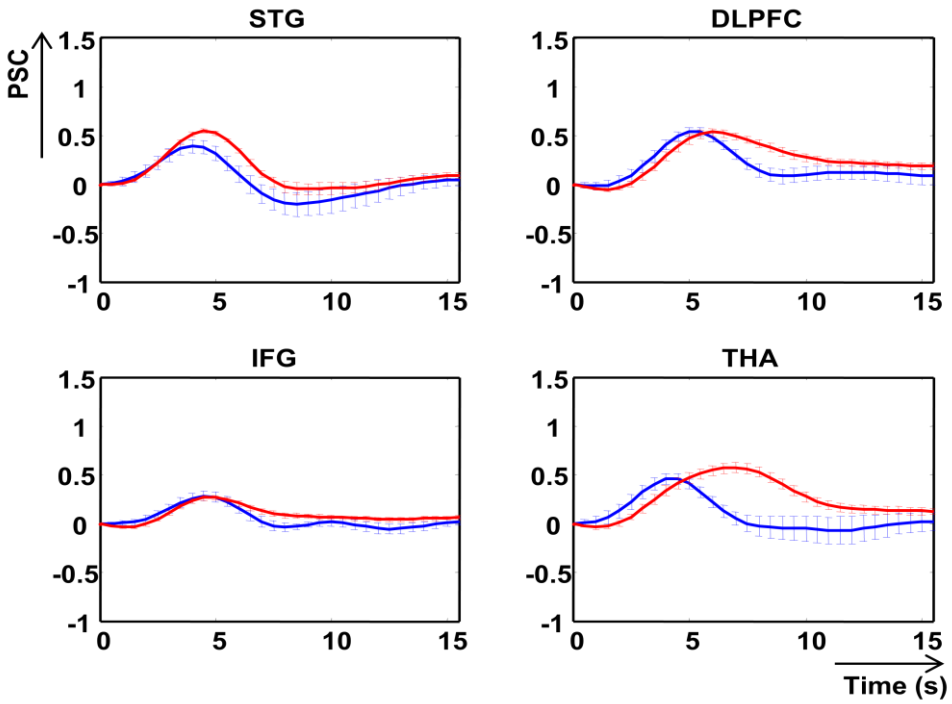

Figure 5.2: Grand averages of the HRFs for single stimuli (blue curve) and HRFs for double stimuli (red curve) for each ROI. Error bars represent standard deviations across the 14 sample subjects.

Given the rather small responses seen for some ROIs, we further examined the THA's subject-specific templates for the single and double stimuli shown in Figure 5.3.

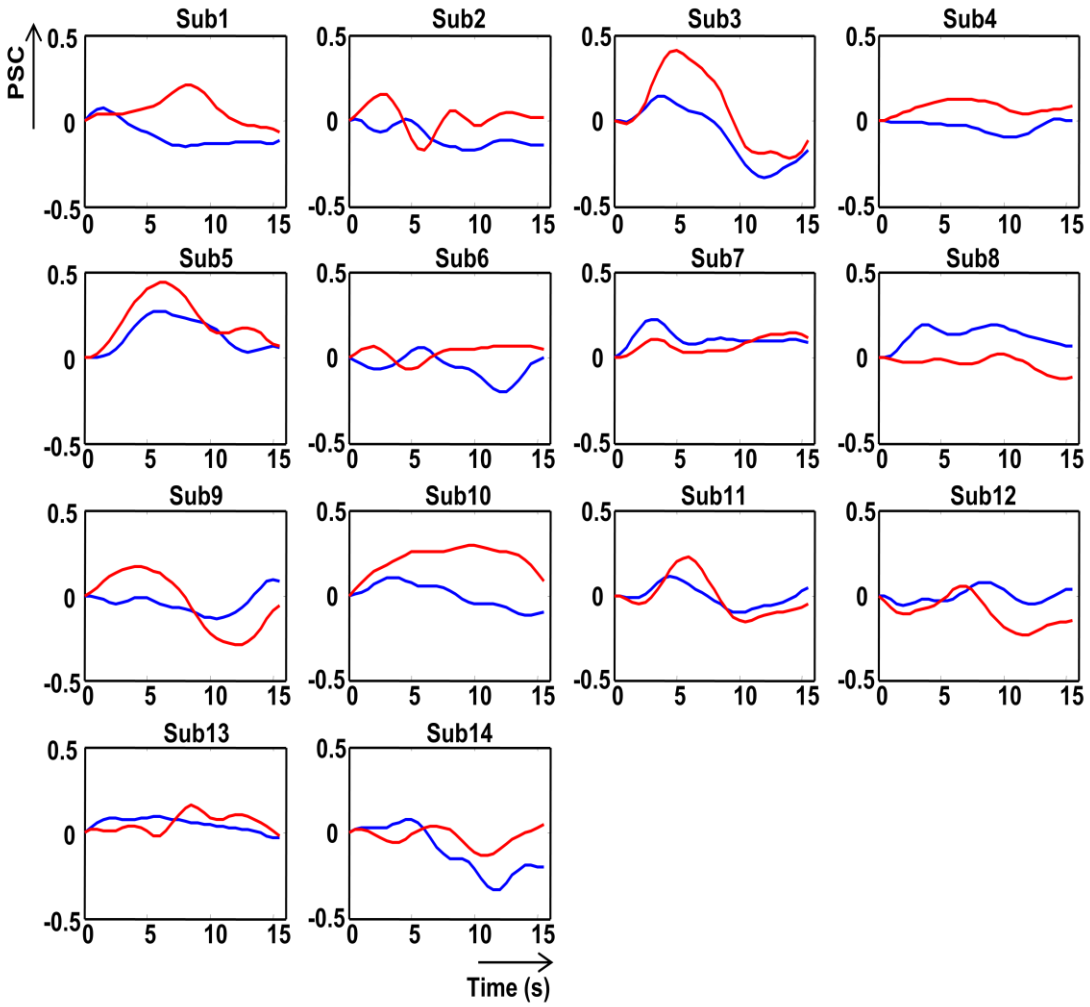

Figure 5.3: The template for single (blue) and double (red) stimuli for each subject for THA.

Figure 5.3 shows that large variability exists in the templates across all the subjects with several subjects not showing a clear response to the stimuli (for example subjects 2, 4, 6, 8, 10 and 13). Similar observations were made for

the other ROIs, calling into question the use of subject-specific templates. Therefore, for the remainder of this study, we decided to use the STG template, obtained from the grand-averaged responses to single stimuli. Since the DLPFC, IFG and THA have smaller responses as the STG, the standard deviation threshold was adjusted for these ROIs in proportion to the peak amplitude (see Table 5.1). The grand average (across 14 subjects) of the Active-Estimated HRFs (green curve), the Active-Observed HRFs (red curve) and the HRFs for the active single stimuli (blue curve) obtained from the four ROIs are presented in Figure 5.4. As one can see, comparing Figure 5.4 with Figure 5.2, the peak latency differences between single tone and double tone responses have been largely resolved.

Table 5.1: The peak amplitude for each template, and the proportion of the standard deviation thresholds adjustment in each ROI.

Peak amplitude

	S	D
STG	0.15	0.28
DLPFC	0.03	0.10
IFG	0.04	0.04
THA	0.05	0.09

Proportion

	S	D
DLPFC	4.68	2.71
IFG	3.85	6.65
THA	2.87	2.99

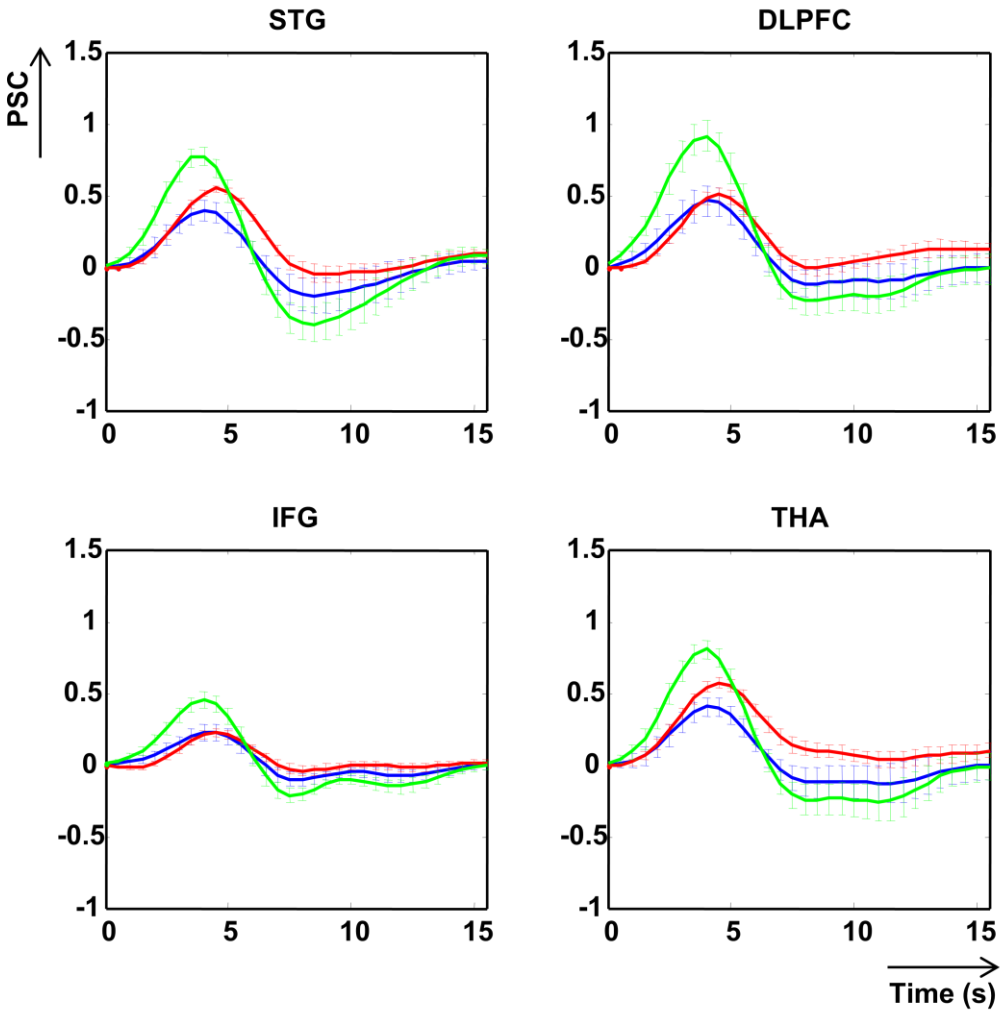

Figure 5.4: Active-Estimated HRF (green), Active-Observed HRF (red) and the HRF for single stimuli (blue) for each ROI using the STG template for single stimuli. Error bars represent standard deviations across the 14 sample subjects.

Two-sided *t*-test were done comparing the peak value of the Active-Estimated HRF and Active-Observed HRF, correcting the *p* values for multiple comparisons using Bonferroni correction, and the results are presented in Table 5.2.

Table 5.2: *T* values and *p* values for comparing the peak value of the Active-Estimated HRF and the Active-Observed HRF for each ROI.

		STG	DLPFC	IFG	THA
A_E	mean	0.77	1.07	0.55	0.91
	sd	0.07	0.04	0.05	0.06
A_O	mean	0.46	0.58	0.23	0.50
	sd	0.02	0.05	0.03	0.05
	df	13	13	13	13
	t	4.391	7.439	5.493	5.463
	p	**0.00073**	**4.91E-06**	**1E-04**	**1E-04**

Table 5.2 shows that the Active-Estimated HRF had significantly larger amplitude than the Active-Observed HRF for all ROIs ($p<0.05$, Bonferroni correction applied) (Table 5.2). The corresponding percentages of active trials were also obtained and are shown in Figure 5.5. A two-sided *t*-test comparing the percentage of active trials for single and double stimuli was performed and the results (Bonferroni correction applied) are listed in Table 5.3.

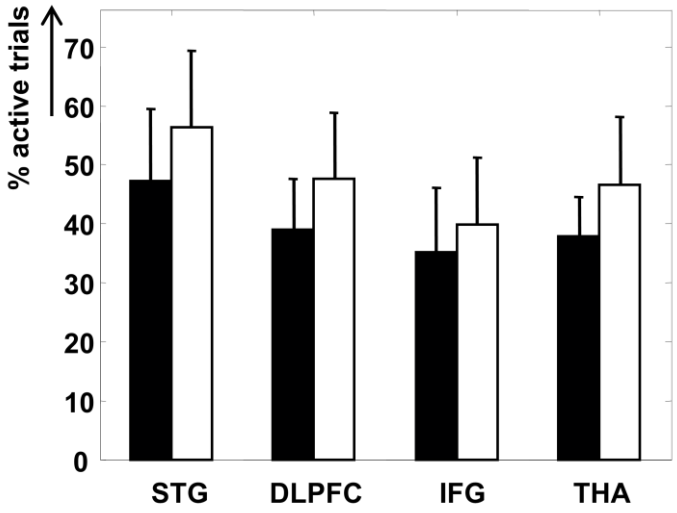

Figure 5.5: The percentages of active trials of STG, DLPFC, IFG and THA for the single stimuli (black) and double stimuli (white).

Table 5.3: *T* values and *p* values for comparing the percentages of active trials in response to double and single stimuli.

		STG	DLPFC	IFG	THA
S	mean	49.21	38.83	35.11	37.9
	sd	12.28	8.768	10.9	6.715
D	mean	56.3	47.66	39.81	46.54
	sd	13.06	11.19	11.38	11.58
	df	13	13	13	13
	t	3.657	2.944	1.323	2.927
	p	**0.003**	**0.011**	0.209	**0.012**

Significant differences were found in STG, DLPFC and THA, but not for IFG. First of all, the results confirm that all the four ROIs responded to single and double stimuli. Recall that we showed in section 3.3.1, that the occipital cortex (OC) only produced 88 active trials out of 566 trials (15.5%), while

these ROIs produced at least two times more active trials than OC (all above 35%).

Combining the finding that all ROIs produced a smaller amplitude Active-Observed HRF than the Active-Estimated HRF, with the observation that only STG, DLPFC and THA produced significantly more active trials for the double stimuli than the single stimuli, leads to the conclusion that STG, DLPFC and THA were responsive to the second stimulus in the paired tone paradigm, but that the hemodynamic responses to the second stimulus was smaller than for the first stimulus in a pair. Thus, this may indicate the involvement of STG, DLPFC and THA in sensory gating. As outlined in Chapter 4, conventional fMRI analysis could not identify the brain areas involved in sensory gating, showing the advantage of our correlation-based method.

To further refine the source of sensory gating, we examined the possible lateralized differences in the peak amplitude of the Active-Estimated HRFs and the Active-Observed HRF, and in the number of active trials for STG, DLPFC, IFG and THA by dividing each ROI into a right side and a left side.

First, the lateralized Active-Estimated HRFs and the Active-Observed HRFs are presented in Figure 5.6 for each ROI. The mean, standard deviation and degree of freedom for the peak values of the Active-Estimated HRF and the Active-Observed HRF are presented in Table 5.4. Two-sided *t*-test on the peak value of Active-Estimated HRF and Active-Observed HRF was done for

each ROI, *p* values were corrected for multiple comparisons using Bonferroni correction and the results are presented in the Table 5.5.

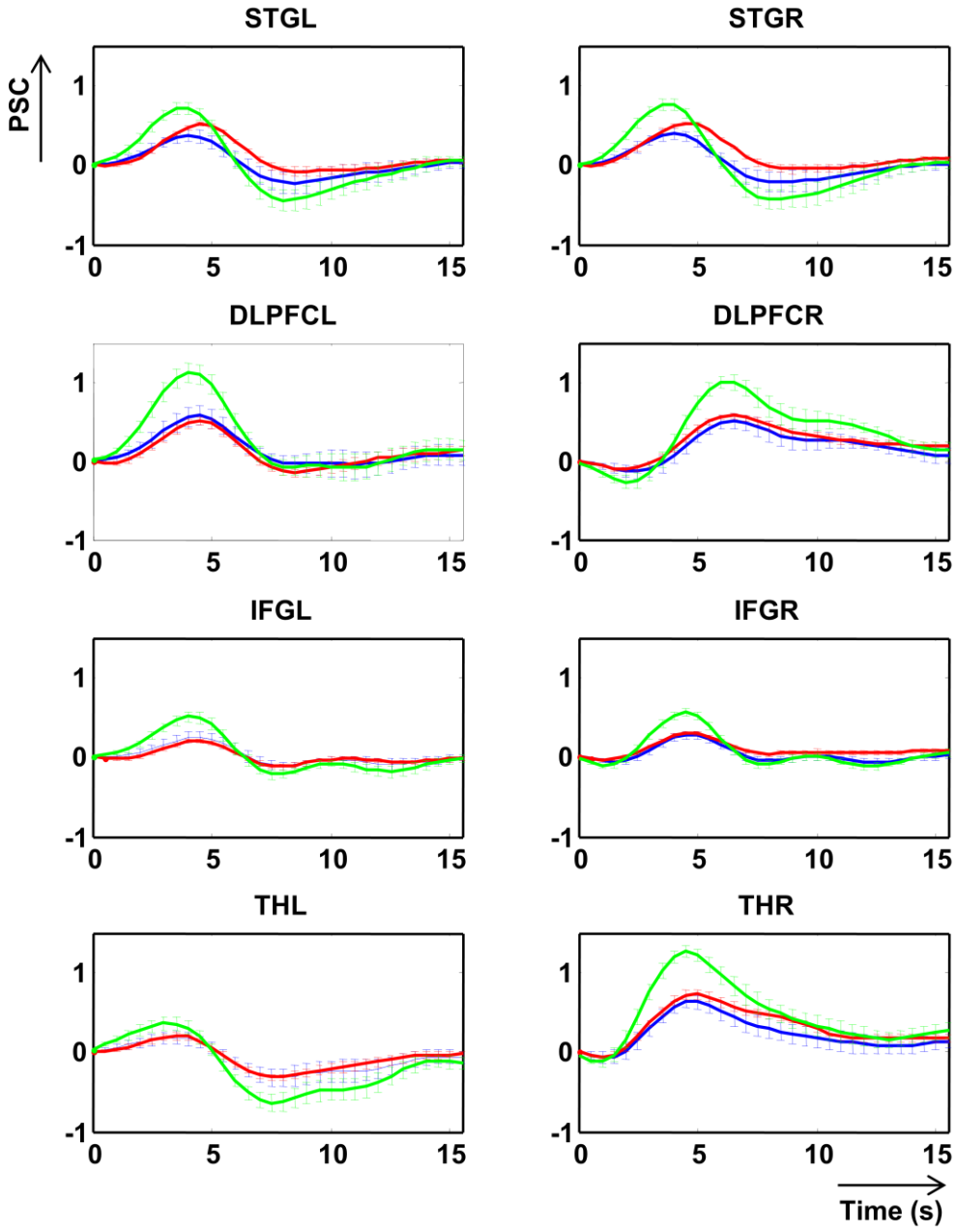

Figure 5.6: Active-Estimated HRF (green), Active-Observed HRF (red) and the HRF for single stimuli (blue) for each ROI using the STG template for single stimuli. Error bars represent standard deviations across the 14 sample subjects.

Table 5.4: Mean, standard deviation (sd) and degree of freedom (df) for the peak value of the Active-Estimated HRF and the Active-Observed HRF for each left and right ROI.

		STG		DLPFC		IFG		THA	
		L	R	L	R	L	R	L	R
A_E	m	0.79	0.77	1.13	1.02	0.51	0.56	0.36	1.26
	sd	0.08	0.07	0.12	0.09	0.06	0.05	0.08	0.07
A_O	m	0.47	0.49	0.51	0.56	0.20	0.31	0.20	0.73
	sd	0.03	0.02	0.06	0.04	0.03	0.02	0.04	0.06
	df	13	13	13	13	13	13	13	13

Table 5.5: *T* values and *p* values for peak value of the Active-Estimated HRF and the Active-Observed HRF for each left and right ROI.

		STG		DLPFC		IFG		THA	
		L	R	L	R	L	R	L	R
E vs O	*t*	3.754	3.866	4.576	4.732	4.393	4.966	1.728	5.598
	p	**0.002**	**0.002**	**5E-04**	**4E-04**	**7E-04**	**3E-04**	0.108	**9E-05**

The results show that the amplitude of the Active-Estimated HRF was significantly larger than for the Active-Estimated HRF for all eight ROIs, except for the left THA ($p<0.05$, Bonferroni correction applied).

Next, the corresponding percentages of active trials for each ROI are presented in Figure 5.7. The mean, standard deviation and degree of freedom of the percentages of active trials for the single and double stimuli for each ROI are presented in Table 5.6. Two-sided *t*-test comparing the percentage of active trials for the single and double stimuli for each ROI was done and the results are listed in Table 5.7.

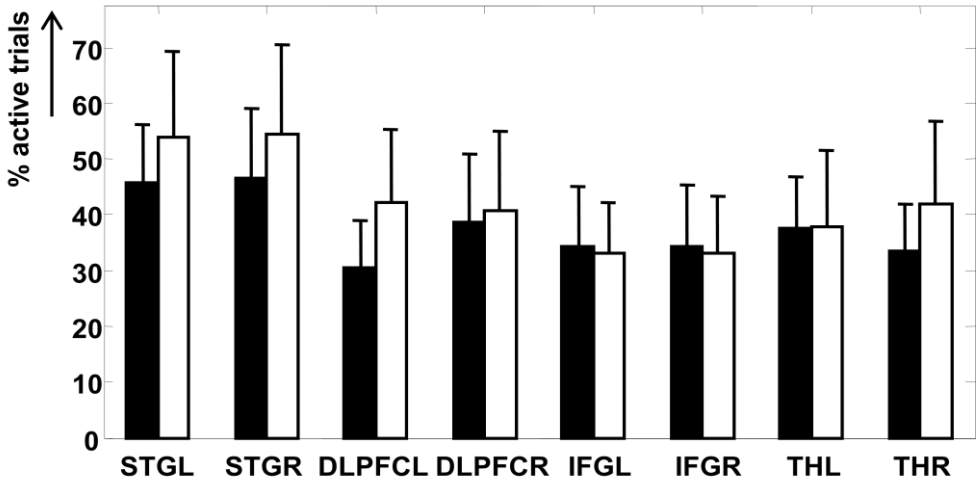

Figure 5.7: The percentages of active trials in the left and right STG, DLPFC, IFG and THA for single and double stimuli (Black: single; White: double).

Table 5.6: Mean, standard deviation (sd) and degree of freedom (df) of the percentages of active trials for the single and double stimuli for each ROI

		STG		DLPFC		IFG		THA	
		L	R	L	R	L	R	L	R
S	m	45.75	46.51	30.60	38.66	34.16	34.33	37.60	33.50
	sd	10.56	12.50	8.27	12.34	10.82	11.18	9.22	8.42
D	m	53.84	55.97	42.06	40.81	33.05	33.15	37.76	41.97
	sd	15.37	14.36	13.20	14.20	8.99	10.28	13.69	14.94
	df	13	13	13	13	13	13	13	13

Table 5.7: *T* values and *p* values for comparing the percentage of active trials for single and double stimuli for each ROI.

	STG		DLPFC		IFG		THA	
S vs. D	L	R	L	R	L	R	L	R
t	3.578	3.725	3.983	0.675	0.424	0.356	0.110	2.996
p	**0.003**	**0.003**	**0.002**	0.511	0.679	0.727	0.914	**0.010**

Significant differences were found in the left and right STG, left DLPFC and right THA. The amplitude analysis and the percentage of active trial analysis, point to an involvement of the bilateral STG, left DLPFC and right THA in sensory gating. We also compared the percentage of active trials between the left side and right side ROI. Two-sided *t*-test were done for the single stimuli and the double stimuli for each ROI and the *p* values for each comparison are summarized in Table 5.8.

Table 5.8: *T* values and *p* values for comparing the percentage of active trials between the left side and right side ROI for single and double stimuli.

	STG		DLPFC		IFG		THA	
L VS. R	S	D	S	D	S	D	S	D
t	0.176	0.364	2.706	0.077	0.011	0.086	2.171	0.686
p	0.863	0.722	**0.018**	0.94	0.991	0.933	**0.049**	0.505

Significant differences were found in the DLPFC and THA for the single stimuli. However, those *p* values did not reach significant after Bonferroni correction was applied. The analysis above showed that neither the right nor left hemisphere STG presented priority in processing single or double stimuli. This result indicates normal involvement of auditory processing in both hemispheres in the healthy subjects.

The results also showed that left hemisphere of the DLPFC responded to single stimuli less frequently than its right counterpart, while no significant difference was found for the double stimuli. This indicates that the left hemisphere was responsive to the double stimuli as frequently as the right

hemisphere. This result further confirmed that the left DLPFC plays an important role in sensory gating.

Also, the right THA showed significantly smaller number of active trials than the left hemisphere for the single stimuli. However, no significant difference between the left and right THA for the double stimuli was found. This result confirmed that the right THA played an important role in sensory gating.

Compared to the results of the conventional analysis, it appears that the correlation-based method uncovers additional information and it appears to have a higher resolving power.

5.3.2 String-based analysis

Here we reanalyze the data once more using the string-based analysis. Section 5.3.1 suggests the involvement of sensory gating in DLPFC and THA. From the literature we know that the STG represents the auditory stimuli processing station, the thalamus processes and relays sensory information to the auditory cortex and DLPFC provides inhibitory modulation of the auditory cortex. Also, the DLPFC has been shown to have extensive connections with the STG (Romanski et al., 1999). Therefore, in this section, we will use the string-based analysis on these areas only. In each string, the first digit represents STG, the second digit represents DLPFC, and the third represents THA. Eight string categories are possible, ranging from 100 to 111. The same sensory gating paradigm was used (Estimated HRF versus Observed HRF) as used in 4.3.1.2.

Figure 5.8 presents the Active-Estimated HRF (blue curve) and Active-Observed HRF (red curve) of the double stimulus responses for each ROI for category “100” through “111”. The two-sided *t* test was done comparing the peak amplitudes between Active-Estimated HRFs and Active-Observed HRFs for each category, the *t* value and *p* value of active groups are presented in the Table 5.9.

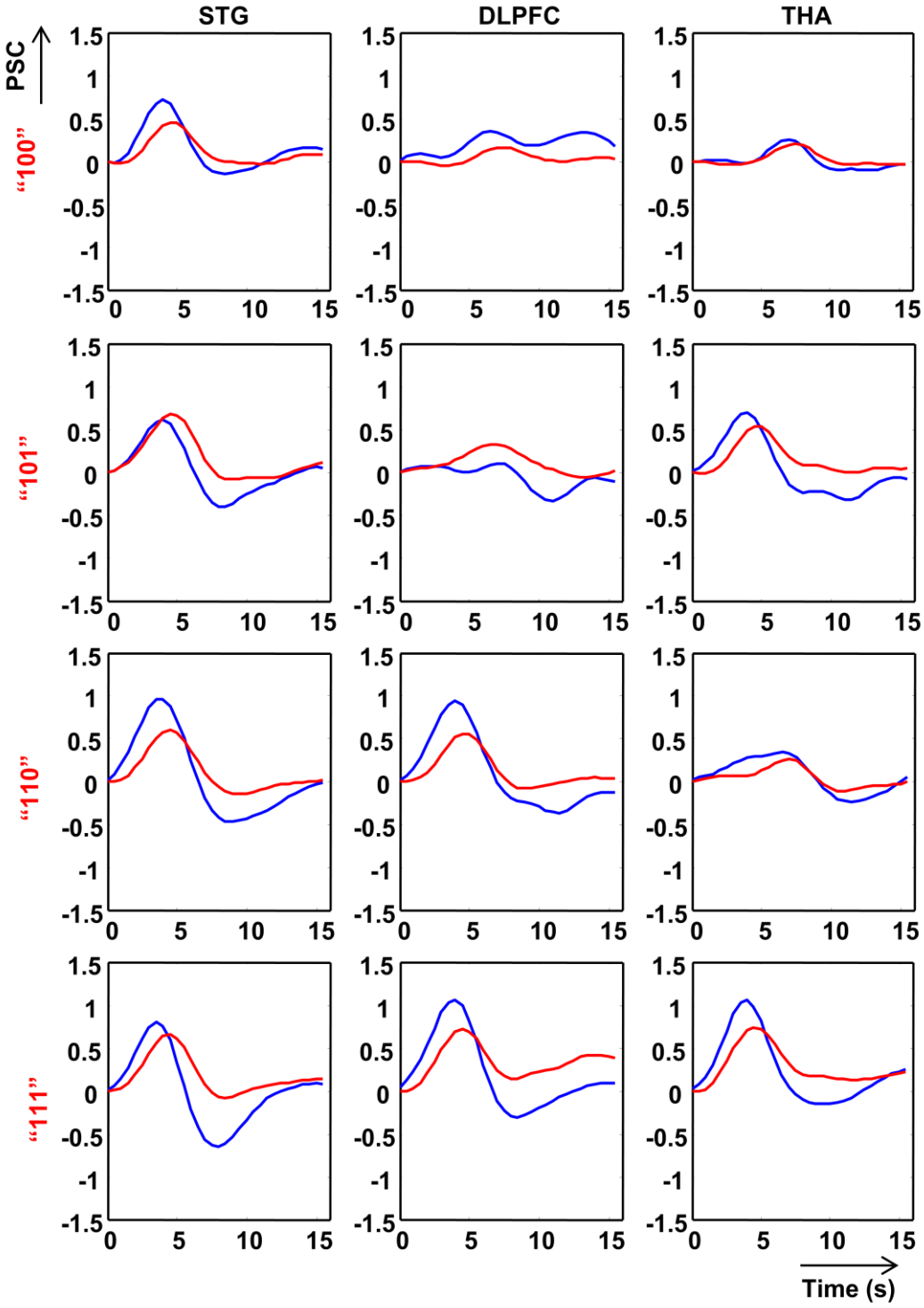

Figure 5.8 (continued): Active-Estimated HRF (blue curve) and Active-Observed HRF (red curve) for each ROI for category "100" (STG: NA, DLPFC: NA, and THA: NA), through "111", (STG: A, DLPFC: A, and THA: A).

Table 5.9: *T* values and *p* values of the peak amplitudes for Active-Estimated HRFs and Active-Observed HRFs for all active categories.

T		STG	DLPFC	THA
100	*t*	5.01	NA	NA
	p	0.0002	NA	NA
101	*t*	0.96	NA	1.71
	p	0.35	NA	0.111
110	*t*	4.71	4.74	NA
	p	0.0004	0.0004	NA
111	*t*	1.82	3.81	3.66
	p	0.09	0.002	0.003

Please note that the DLPFC in Figure 5.8 categories “101” was considered inactive, even though the Active-Observed HRF of the double stimuli shows a late response peaking at 7 s. The reason this group of trials was not classified as active is that we used a windowed template from 2 s to 8 s, and only trials that have a high correlation with this template (and have large variance) will be classified as active trials. In this case, the late response was primarily outside the window considered and thus not classified as active.

We found significant differences between Active-Estimated HRFs and Active-Observed HRFs for DLPFC and THA in all categories ($p<0.05$). This further supported the previous results (Section 5.3.1). STG indicated the existence of two patterns, in category “100” and “110”, no significant difference was found, while in category “101” and “111”, a significant difference was found. A clear interaction between STG and THA can also be observed; when THA is non-active, STG shows similar peak amplitudes for the Estimated HRFs and the observed HRFs, but when THA is active, STG shows greater peak amplitude for the Estimated HRFs than the observed HRFs.

The corresponding percentage of active trials for the single and double stimuli in categories “000” to “111” are summarized in Figure 5.9. The results of the two-sided *t*-test comparing the percentage of active trials for the single and the double stimuli for each category are presented in the Table 5.10.

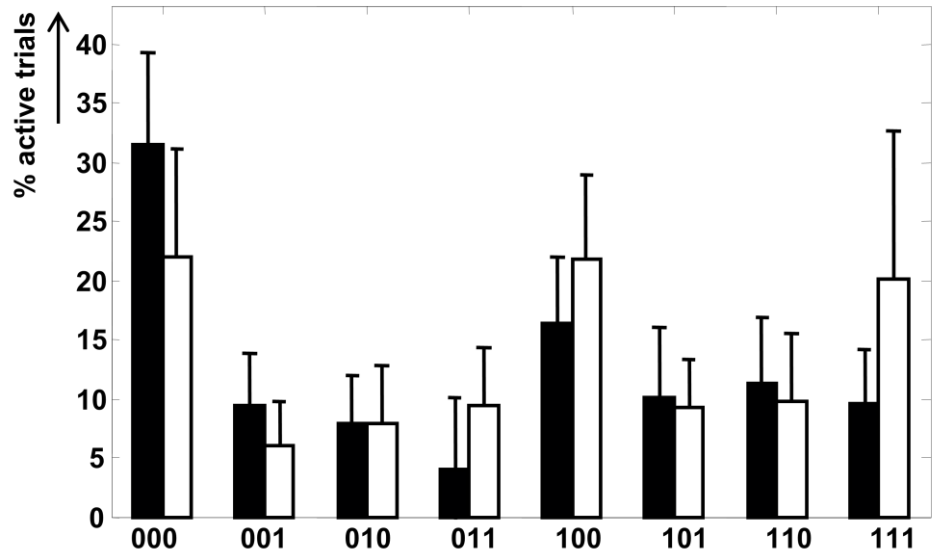

Figure 5.9: The percentages of active trials for the single (black) and double (white) stimuli in categories “000” to “111”.

Table 5.10: *T* values and *p* values for comparing the percentage of active trials for the single and double stimuli for each category.

		000	001	010	011	100	101	110	111
	m	31.46	9.39	7.95	4.02	16.35	10.06	11.22	9.55
S	sd	7.83	4.40	4.07	6.08	5.57	5.95	5.71	4.55
	m	21.93	6.00	7.86	9.34	15.71	9.24	9.81	20.10
D	sd	9.11	3.69	4.98	5.05	5.80	4.07	5.70	12.51
	df	13	13	13	13	13	13	13	13
	t	3.59	1.92	0.05	2.44	3.88	0.52	0.64	3.47
	p	**0.003**	0.075	0.957	**0.029**	**0.002**	0.609	0.534	**0.004**

The results showed that the single stimuli produced significantly more active trials than the double stimuli in category “000” (t=3.59, p=0.003, df=13), and the double stimuli produced significantly more active trials than the single stimuli in category “011” (t=-2.44, p=0.029, df=13), category “100” (t=3.88, p=0.001, df=13), and category “111” (t=-3.47, p=0.004, df=13).

In summary, several results were found using the string-based method: first, we verified that the THA and the DLPFC showed suppressed responses for the observed HRF than the Estimated HRF in all categories which confirmed the involvement of sensory gating in these ROIs. Second, a clear interaction between STG and THA was found. Third, we found three categories (“011”, “100” and “111”) were more prevalent for double stimuli than the single stimuli.

5.4 Conclusion

To our knowledge, this was the first event-related fMRI study to examine cortical regions that are involved in sensory gating using single trial analysis in healthy subjects during a classical sensory gating paradigm. In this chapter, we applied the correlation-based method to examine sensory gating and confirmed the involvement of STG, THA and DLPFC in sensory gating. The lateralization analysis provided additional information that only the bilateral STG, left DLPFC and right THA were involved in gating.

Thalamic involvement in sensory gating has been suggested in prior animal studies (Hinman et al., 1983; Erwin et al., 1987), as well as fMRI studies (Mayer et al., 2009; Tregellas et al., 2007). In addition to THA

involvement, our results indicated that sensory gating may also occur in the DLPFC. Previous evidence of DLPFC's involvement in gating has been reported in surface and intracranial recordings (Knight et al., 1999; Grunwald et al., 2003) as well as two fMRI studies (Tregellas et al., 2007; Mayer et al., 2009). In addition, STG involvement in gating has been reported by Mayer et al., (2009). Our results also support Mayer's findings. Finally, the involvement of HPC in sensory gating is still under debate in fMRI studies. Tregellas et al., (2007) found evidence of gating in HPC, but they used a train of clicks instead of classic pairs of tones. In contrast, (Mayer et al., 2009) applied the classic double tone paradigm and they did not find HPC involvement in both processing single or double tones. Our results did not find HPC involvement which further support Mayer's finding.

Grunwald et al. (2003) proposed a sensory gating model which indicated that the STG processes the basic stimulus properties during the first stage of auditory sensory gating. Whereas the PFC further inhibit the sensory information flow within the cortex. Our lateralization analysis provides additional information that the right THA relayed the sensory signal to STG in healthy subjects. Then, the bilateral STG is involved in the first stage of auditory processing. Finally, the left DLPFC may be involved in the inhibitory circuit of sensory gating processing.

Compared with conventional fMRI analysis, the correlation-based single trial analysis provides quantitative assessment of the neuronal origins of the sensory gating and offers additional information.

Chapter 6: Discussion and Future work

6.1 Discussion and Conclusions

We introduced a correlation-based single trial analysis method for the analysis of auditory fMRI data. This method provides a way to remove the non-active trials and thus improving the sensitivity of the statistical analysis.

This method goes beyond existing approaches aimed at improving the analysis of BOLD fMRI data including the parametric methods such as canonical HRF and its partial derivatives (Friston et al., 1998) and the non-parametric methods such as averaging method (Kang et al., 2003), deconvolution method (Lu et al., 2006, Wink et al., 2008), principal component analysis-PCA (Hossein et al., 2003), and the Bayesian method (Ciuciu et al., 2003; Marrelec et al., 2003).

The correlation-based method developed here has the advantages that it is data-driven instead of model-driven and it does not rely on any assumptions regarding the HRF. In the case of parametric methods, these functions are usually selected prior to the analysis and fixed over time and through brain regions. In the correlation-based method, the extracted HRFs are determined only by the fMRI signal and the stimuli, and they are not biased by any a priori model.

The correlation-based method also has the advantage that no rough approximation is needed. In contrast, the PCA method (Hossein et al., 2003) requires the signal to be transformed into several orthogonal components, with the first few components (with the largest eigenvalues) selected to model

the HRF. However, the maximum-variance variables may not always maximize information and using the first few components may not able to capture the true response. In the case of the averaging method (Kang et al., 2003), the subject-specific HRF is obtained by projecting the actual fMRI signal onto a Fourier basis which is probably only a rough approximation of the BOLD response. Our correlation-based method uses a template, derived from the data (essentially the ensemble average across all responses), to measure the similarity between the template and all trials. The subject-specific HRFs are then obtained by averaging the active trials. Thus, our method does not require the a priori estimation of the HRF.

Furthermore, the correlation-based method has the advantages that only two parameters need to be selected; the correlation threshold, and the standard deviation threshold. In contrast, four parameters are needed using the canonical HRF and its partial derivatives (Friston et al., 1998). In the case of the deconvolution method (Lu et al., 2006), the number of parameters is 35, and all the parameters have to be manually selected to improve the fit of the model.

Also, in the correlation-based method, no assumption is made that all the single trials are the same. The problem with methods such as the Bayesian method is that it is often assumed that the HRFs are identical from one response to another which is unlikely to be the case (Aguirre et al., 1998). The correlation-based method quantifies the single-trial variability, thus it can capture all different kinds of HRFs that may exist during an experiment. Hence, it provides a great deal of flexibility and variability in the type of

response that can be detected. In addition, this method has the advantage of simplicity compared to the methods described above.

Several limitations of the current study should be considered. First, we have to pre-define ROIs to extract the single trials. We reviewed the SPM produced using the canonical HRF, and the main areas of activation were selected. So the subject-specific HRFs were unlikely to differ a lot from the canonical HRF. Therefore, this approach may be biased toward activated regions that have a HRF similar to the canonical HRF.

Second, it should also be noted that this approach seems to overfit the data and be biased since the AS-HRFs were obtained from the data itself and could match the data more accurately. However, both the correlation-based method and the conventional analysis using canonical HRF use the least squares method to estimate the parameters β (equation A1-7). So the comparison between the subject-specific HRF and the canonical HRF is unbiased.

Third, we evaluated the performance of the correlation-based method on simulated data. The data were generated using data obtained from an auditory experiment. The 0 s to 8 s interval of each trial following the stimulus presentation was used as active responses, and the 8 s to 16 s intervals were used as “non-active” responses. However, many of the hemodynamic responses exhibit a (small) undershoot in the 8 s to 16 s intervals. This results in a tendency to have negative-amplitude responses in the “non-active” group, thus potentially biasing the clustering results. In future tests, one may consider using data from non-active ROIs.

The ability of the correlation-based method for detecting brain activation was demonstrated on real fMRI data in healthy subjects listening to single tones. The same data was also analyzed using the conventional fMRI analysis which applied canonical HRF. It was found that the HRF obtained with the correlation-based method had the best goodness of fit (R) of the model to the data in all subjects. Also, the AS-HRF-based SPM increased detection sensitivity as compared to the C-HRF-based SPM and thus could delineate more precisely the activated areas. This comparison analysis confirmed the improvement of the SPM processing using the new method.

The correlation-based method was also applied to investigate sensory gating network. While the conventional analysis could not find any regions involved in gating, the correlation-based method provides quantitative assessment of the neuronal origins of sensory gating and provided additional information that the right THA and left DLPFC were involved in sensory gating.

Our research showed that only 51% of the responses in the auditory cortex were active. This result is consistent with electrophysiological studies that show that not all stimuli produce evoked potentials in healthy subjects (Hu et al., 2009). The inconsistency of the response in time may due to the physiological or neural adaptation to the stimuli, since one must collect many trials and the subjects become adapted to the stimuli and may not respond anymore. It is also possible that true active responses are buried in the noise and cannot captured using the correlation-based method. As a matter of fact, a simulation was conducted to test how big a percentage of true active responses could be detected at different SNR, and the results showed that

only 80% of true active responses among all the “active” responses could be identified at SNR 0.2. Therefore, we should keep in mind that the correlation-based method still misclassified some non-active trials into the active group due to the low SNR in fMRI data. To test the feasibility of this method, we compared the percentage of active trials obtained from active brain regions (AC) and non-active regions (OC). The correlation-based method detected significantly more active trials in AC than OC. So, it is potentially a powerful exploratory method.

To our knowledge, there is no other single trial analysis of auditory fMRI data has been done. The objective of this study was to introduce the correlation-based method to the fMRI data analysis field. Compared with the conventional technique, the correlation-based technique increased detection sensitivity. By applying this new proposed method to investigate sensory gating, additional information can be obtained.

6.2 Future Work

The correlation-based method used the AS-HRF which obtained from STG only. However, variability of HRF has been observed from different brain regions within the same subject. Future studies might seek to address whether the Active Region-Specific or Voxel-Specific HRF can improve the current method.

In this study, we did not use anatomical masks for the group level activation maps. Therefore, the activation regions shown in Table 4.1 and 4.2 contain voxels that are not part of the anatomically-defined STG, IFG, DLPFC

or THA. For example, the single stimuli activated 317 voxels in the greater STG area, however, only 189 of these were STG, with the others situated in the postcentral gyrus, insula, middle temporal gyrus, inferior parietal lobule, extra-nuclear, etc.. We suggest that if using the group-level SPM, the anatomical mask could be used to identify ROIs precisely.

Also, some studies have shown that these group-level ROIs are not as reliable as the individually-created ones (Swallow et al. 2003) since it does not take into account the inter-individual functional variability. This issue could be addressed by using individual-level ROIs. Another application of the correlation-based method is to study patient populations, e.g., schizophrenia patients. One problem in fMRI data analysis of patients is that a significant proportion of the patients do not show any activation (Krakow et al., 2001). Potential reasons may lie in the large variability of the HRFs, and the shape of patient-specific HRF could be significantly different from healthy subjects. In the future, we could apply the correlation-based method on activation detection of patients with schizophrenia in order to see if the detection sensitivity can be increased by using the patient-specific HRF. Lastly, to confirm that the correlation-based method can differentiate between active and non-active trials, simultaneous EEG/fMRI studies need to be conducted. One would expect to see no BOLD signal if the electrophysiological response is absent. Also, such a study may be used to determine if an electrophysiological response is putatively associated with a BOLD response. For example, if a stimulus results in additive neural activity, a BOLD response should be seen as well. However, if the response to a stimulus is primarily

dues to phase reorganization of the ongoing activity, no BOLD response may be seen.

References

Adler LE, Pachtman E, Franks RD, Pecevich M, Waldo MC, Freedman R (1982): “Neurophysiological evidence for a defect in neuronal mechanisms involved in sensory gating in schizophrenia.” *Biol Psychiatry*, 17, 639-654.

Adler LE, Waldo MC, Thatcher A, Cawthra E, Baker N, Freedman R (1990): “Lack of relationship of auditory gating defects to negative symptoms in schizophrenia.” *Schizophrenia Research*, 3, 131-138.

Aguirre GK, Zarahn E, D’Esposito M (1998): “The variability of human, BOLD hemodynamic responses.” *Neuroimage*, 8 (4), 360– 369.

Anders M, Dale RLB (1997): “Selective averaging of rapidly presented individual trials using fMRI.” *Human Brain Mapping*, 5, 329-340.

Boutros NN, Zouridakis G, Overall J (1991): “Replication and extension of P50 findings in schizophrenia.” *Clinical Electroencephalogram*, 22(1), 40-5.

Boutros NN, Trautner P, Rosburg T, Korzyukov O, Grunwald T, Schaller C, Elger CE, Kurthen M (2005): “Sensory gating in the human hippocampal and rhinal regions.” *Clinical Neurophysiology*, 116, 1976-1974.

Boynton G, Engel S, Glover G, Heeger D (1996): “Linear systems analysis of functional magnetic resonance imaging in human.” *Vl. J. Neuroscience*, 16, 4207–4221.

Brodtmann A, Puce A, Darby D, Donnan G (2007): “fMRI demonstrates diaschisis in the extrastriate visual cortex.” *Stroke*, 38 (8), 2360–2363.

Buckner RL, Peter AB, Kathleen MO, Robert LS, Steven EP, Marcus ER, Bruce RR (1996): “Detection of cortical activation during averaged single trials of a cognitive task using functiona magnetic resonance imaging.” *Proceedings National Academy of Sciences*, 93 (25), 14878-14883.

Buxton RB (2002): Introduction to Functional Magnetic Resonance Imaging: Principles and Techniques. Cambridge University Press, New York.

Carey J, Kimberley T, Lewis S, Auerbach E, Dorsey L, Rundquist P, Ugurbil K (2002): “Analysis of fMRI and finger tracking training in subjects with chronic stroke.” *Brain*, 125, 773–788.

Ciuciu P, Poline JB, Marrelec G, Idier J, Pallier C, Benali H (2003): “Unsupervised robust nonparametric estimation of the hemodynamic response function for any fMRI experiment.” *IEEE Trans. Medical Imaging*, 2022 (10), 1235-1251.

Erwin RJ, Buchwald JS (1987): “Midlatency auditory evoked responses in the human and the cat model.” *Electroencephalogr. Clin. Neurophysiol., Suppl.,* 40, 461–467.

Freedman R, Waldo M, Bickford-Wimer P, Nagamoto H (1991): “Elementary neuronal dysfunctions in schizophrenia.” *Schizophr. Res*., 4, 233–243.

Friston KJ, Jezzard P, Turner R (1994): “Analysis of functional MRI time-series.” *Human Brain Mapping*, 1, 153–171.

Friston KJ, Holmes A, Poline J, Grasby P, Williams S, Frackowiak R, Turner R (1995): “Analysis of fMRI time-series revisited.” *NeuroImage*, 2 (1), 45–53.

Friston KJ, Fletcher P, Josephs O, Holmes AP, Rugg MD, Tumer R (1998): “Event-related fMRI: characterizing differential responses.” *NeuroImage*, 7, 30-40.

Gossl C, Auer DP, Fahrmeir L (2001): “Bayesian spatiotemporal inference in functional magnetic resonance imaging.” *Biometrics*, 57, 554– 562.

Grunwald T, Boutro NN, Pezera N, von Oertzen J, Fernández G, Schaller C, Elger CE (2003): “Neuronal substrates of sensory gating within the human brain.” *Biological Psychiatry,* 53 (6), 511-519.

Hinman CL, Buchwald JS (1983): “Depth evoked potential and single unit correlates of vertex midlatency auditory evoked responses.” *Brain Research*, 264, 57–67.

Handwerker D, Ollinger J, D'Esposito M (2004): “Variation of BOLD hemodynamic responses across subjects and brain regions and their effects on statistical analyses.” *NeuroImage,* 21, 1639–1651.

Heller R, Stanley D, Yekutieli D, Rubin N, and Benjaminia Y, (2006): “Cluster-based analysis of FMRI data.” *NeuroImag*e, 33, 599–608.

Hossein-Zadeh GA, Ardekani BA, Soltanian-Zadeh H (2003): “Signal subspace approach for modeling the hemodynamic response function in fMRI.” *Magnetic Resonance Imaging*, 21, 835–843.

Huettel SA, Song AW, McCarthy G (2004): Functional Magnetic Resonance Imaging. Sinauer Associates.

Inan S, Mitchell T, Song A, Bizzell J, Belger A (2004): “Hemodynamic correlates of stimulus repetition in the visual and auditory cortices: an fMRI study.” *NeuroImag*e, 21, 886-893

Josephs O, Turner R, Friston K (1997): “Event-related fMRI.” *Hum. Brain Mapp.*, 5 (4), 243–248.

Kang JK, Benar CG, Asmi AA, Khani YA, Pike GB, Dubeau F, Gotman J (2003): “Using patient-specific hemodynamic response functions in combined EEG-fMRI studies in epilepsy.” *Neuroimage*, 20, 1162-1170.

Kim SG, Richter W, Ugurbil K (1997): “Limitations of temporal resolution in functional MRI.” *Magn. Reson. Med.*, 37, 631–636.

Knight RT, Scabini D, Woods DL (1989): “Prefrontal cortex gating of auditory transmission in humans.” *Brain Res.*, 504, 338-342.

Knight RT, Staines WR, Swick D, Chao LL (1999): “Prefrontal cortex regulates inhibition and excitation in distributed neural networks.” *Acta Psychol. (Amst)*, 101, 159–178.

Korzyukov O, Pflieger ME, Wagner M, Bowyer SM, Rosburg T, Sundaresan K, Elger CE, Boutros NN, (2007): “Generators of the intracranial P50 response in auditory sensory gating.” *Neuroimage*, 35, 814–826.

Krakow K, Lemieux L, Messina D, Scott CA, Symms MR, Duncan JS, Fish DR (2001): “Spatio-temporal imaging of focal interictal epileptiform activity using EEG-triggered functional MRI.” *Epileptic Disord.*, 3 (2), 67– 74.

Levin JM, Ross MH, Mendelson JH, Kaufman MJ, Lange N, Maas LC, Mello NK, Cohen BM, Renshaw PF (1998): “Reduction in BOLD fMRI response to primary visual stimulation following alcohol ingestion.” *Psychiatry Res.*, 82 (3), 135– 146.

Lu Y, Bagshaw AP, Grova C, Kobayashi E, Dubeau F, Gotman J (2006): “Using voxel-specific hemodynamic response function in EEG-fMRI data analysis.” *Neuroimage*, 32, 238-247.

Luft A, Smith G, Forrester L, Whitall J, Macko R, Hauser T, Goldberg A, Hanley D (2002): “Comparing brain activation associated with isolated upper and lower limb movement across corresponding joints.” *Hum. Brain Mapp.*, 17 (2), 131–140.

Marrelec G, Benali H, Ciuciu P, Pélégrini-Issac M, Poline JB (2003): “Robust Bayesan estimation of the hemodynamic response function in event-related BOLD fMRI using basic physiological information.” *Hum. Brain Mapp.*, 19(1), 1-17.

Mayer AR, Hanlon FM, Franco AR, Teshiba TM, Thoma RJ, Clark VP, Canive JM (2009): “The neural networks underlying auditory sensory gating.” *Neuroimage*, 44, 182-189.

Menz MM, Neumann J, Muller K, Zysset S (2006): “Variability of the BOLD response over time: an examination of within-session differences.” *NeuroImage*, 32, 1185-1194.

Miezin F, Maccotta L, Ollinger J, Petersen S, Buckner R (2000): “Characterizing the hemodynamic response: effects of presentation rate, sampling procedure, and the possibility of ordering brain activity based on relative timing.” *NeuroImage*, 11, 735–759.

Romanski LM, Tian B, Fritz J, Mishkin M, Goldman-Rakic PS, Rauschecker JP (1999): “Dual streams of auditory afferents target multiple domains in the primate prefrontal cortex.” *Nat Neurosci,* 2, 1131–1136.

Neumann J, Lohmann G, Zysset S, von Cramon D (2003): “Within-subject variability of BOLD response dynamics.” *NeuroImage*, 19, 784–796.

Noseworthy MD, Alfonsi J, Bells S (2003): “Attenuation of brain BOLD response following lipid ingestion.” *Hum. Brain Mapp*., 20 (2), 116– 121.

Ogawa S, Lee TM, Kay AR, Tank DW (1990): “Brain magnetic resonance imaging with contrast dependent on blood oxygenation.” *Proc Nat Acad Sci USA*, 87:9868-9872.

Pell GS, Briellmann RS, Chan CHP, Pardoe H. Abbott DF, Jackson GD. (2008): “Selection of the control group for VBM analysis: influence of

covariates, matching and sample size.” *NeuroImage*, 41 (4), 1324–1335.

Plaza M, Gatignol P, Leroy M, Duffau H (2009): “Speaking without Broca's area after tumor resection.” *Neurocase.*, 9, 1-17.

Poldrack RA, Wagner AD, Prull MW, Desmond JE, Glover GH, Gabrieli JD (1999): “Functional specialization for semantic and phonological processing in the left inferior prefrontal cortex.” *Neuroimage*, 10, 15–35.

Poldrack RA (2007): “Region of interest analysis for fMRI.” *Soceity Cogn. Affect. Neuroscience*, 2 (1), 67-70.

Rajapakse JC, Kruggel F, Maisog JM, von Cramon DY (1998): “Modeling hemodynamic response for analysis of functional MRI time-series.” *Human Brain Mapping*, 6, 283– 300.

Swallow KM, Braver TS, Snyder AZ, Speer NK, Zacks JM (2003): “Reliability of functional localization using fMRI.” *Neuroimage*, 20 (3), 1561-77.

Seifritza E, Sallec FD, Espositod F,Herdenera M,Neuhoffe JG, Schefflerf K (2006): “Enhancing BOLD response in the auditory system by neurophysiologically tuned fMRI sequence.” *NeuroImage*, 29 (3), 1013 ‑1022.

Saxe R, Brett M, and Kanwisher N (2006): “Divide and conquer: A defense of functional localizers.” *NeuroImage*, 30, 1088–1096.

Steriade M and Llinas R (1988): “The functional states of the thalamus and the associated neuronal interplay.” *Physiological Reviews*, 68, 699-742.

Thoma RJ, Hanlon FM, Moses SN, Ricker D, Huang M, Edgar C, Irwin J, Torres F, Weisend MP, Adler LE, Miller GA, Canive JM (2005): “M50 sensory gating predicts negative symptoms in schizophrenia.” *Schizophrenia Research*, 73, 311–318.

Tregellas JR, Davalos DB, Rojas DC, Waldo MC, Gibson L, Wylie K, Du YP, Freedman R (2007): “Increased hemodynamic response in the hippocampus, thalamus and prefrontal cortex during abnormal sensory gating in schizophrenia.” *Schizophenia Research*, 92, 262-272.

Wang XF, Jiang Z, Daly JJ, Yue GH (2012): “A generalized regression model for region of interest analysis of fMRI data.” *NeuroImage*, 59(1), 502-510.

Wink AM, Hoogduin H, Roerdink JB (2008): “Data-driven haemodynamic response function ectraction Fourier-wavelet regularized deconvolution.” *BMC Medical Imaging*, 8, 7.

Appendix

A1: First-level analysis

The canonical HRF is given by

$$Y = A(\frac{t^{\alpha_1 - 1}\beta_1^{\alpha_1}e^{-\beta_1 t}}{gamma(\alpha_1)} - c\frac{t^{\alpha_2 - 1}\beta_2^{\alpha_2}e^{-\beta_2 t}}{gamma(\alpha_2)}) \quad , \qquad \text{(A1-1)}$$

where *t* is the time in seconds, gamma (α) is the standard gamma variate, *A* controls the amplitude, *α* and *β* control the shape and scale, respectively, and *c* determines the size of the undershoot (Friston et al. 1998).

A common way to plot the impulse hemodynamic response is in percentage signal change from a baseline condition. GLM expresses the observed response variable in terms of a linear combination of explanatory variables plus an error term. For a simple model with an explanatory variables x_i, the general linear model can be written as

$$y_i = x_i\beta + \varepsilon_i \ , \qquad \text{(A1-2)}$$

where y_i is the observed value for voxel *i*, *β* is the scaling of the linear regression line, and ε_i is the error term in volume *i*. In the statistical analysis of fMRI, this formula is in essence solved for each voxel in each volume in the fMRI time series separately. If the model includes more variables it is convenient to write the general linear model in matrix form using

$$Y = X\beta + \varepsilon \ , \qquad \text{(A1-3)}$$

where *Y* is a matrix containing all the observed data with a column for each voxel and a row for each fMRI volume, β is the parameter matrix and ε is a matrix of error terms. The matrix *X* is known as the design matrix containing the predicted data. It has one row for each fMRI volume and one column for every explanatory variable in the model. In analyzing an fMRI experiment, the columns of *X* contain vectors corresponding to the 'on' and 'off' elements of the stimulus presented. By finding the magnitude of the parameters in β, we can detect the presence or absence of activation (Friston et al., 1995).

Estimates of the parameters $\hat{\beta}$ are obtained using a least squares method, minimizing the squared error given by

$$S = \sum_j \varepsilon_j^2 = \varepsilon^2 \ . \qquad \text{(A1-4)}$$

To obtain the best possible fit of the model to the data, the “stimulus function” (which is often a sharp on or off waveform) is normally convolved with the standard HRF. The stimulus function is known from the experimental setup. The parameter β can be determined by solving the 'normal equations'

$$X^T Y = (X^T X)\ \hat{\beta} \ . \qquad \text{(A1-5)}$$

Provided that $(X^T X)$ is invertible then $\hat{\beta}$ is given by

$$\hat{\beta} = (X^T X)^{-1} X^T Y \ . \qquad \text{(A1-6)}$$

After determine the error term, statistical inference can be made as to whether the β parameter corresponding to the model of an activation response is significantly different from zero.

To convert a parameter estimate (the estimated β value) into a useful statistic, the *t* statistic is obtained using

$$t = \frac{c^T \hat{\beta}}{\sigma(c^T \hat{\beta}) / \sqrt{N}} \ . \qquad \text{(A1-7)}$$

The vector $c^T = [c_1, c_2, \ldots c_i]$, where *i* is the number of parameters in *X*, is referred to as the contrast vector. The word “contrast” is used for the result of the operation $c^T \hat{\beta}$. The standard error is estimated using the variance of the residuals (σ) divided by the appropriate degrees of freedom ($\sqrt{N}$). If the parameter estimate is low relative to its estimated uncertainty, the fit is not significant. The above process is known as the first-level analysis.